Effect of changing vegetation on denudation (part 1): Predicted vegetation composition and cover over the last 21 thousand years along the Coastal Cordillera of Chile

Christian Werner[1], Manuel Schmid[2], Todd A Ehlers[2], Juan Pablo Fuentes-Espoz[3], Jörg Steinkamp[1],
5 Matthew Forrest[1], Johan Liakka[4], Antonio Maldonado[5], Thomas Hickler[1,6]

[1] Senckenberg Biodiversity and Climate Research Centre (SBiK-F), Senckenberganlage 25, 60325 Frankfurt, Germany
[2] University of Tuebingen, Department of Geosciences, Wilhelmstrasse 56, 72074 Tuebingen, Germany
[3] Department of Silviculture and Nature Conservation, University of Chile, Av. Santa Rosa 11315, La Pintana, Santiago RM,
Chile
10 [4] Nansen Environmental and Remote Sensing Center, Bjerknes Centre for Climate Research, Thormøhlens gate 47, N-5006
Bergen, Norway
[5] Centro de Estudios Avanzados en Zonas Áridas (CEAZA), Raúl Bitrán 1305, La Serena, Chile
[6] Department of Physical Geography, Geosciences, Goethe-University, Altenhoeferallee 1, 60438 Frankfurt, Germany

15 *Correspondence to:* Christian Werner (christian.werner@senckenberg.de)

Abstract

Vegetation is crucial for modulating rates of denudation and landscape evolution as it stabilizes and protects hillslopes and intercepts rainfall. Climate conditions and atmospheric CO_2 concentration ($[CO_2]$) influence the establishment and performance of plants and thus have a direct influence on vegetation cover. In addition, vegetation dynamics (competition

20 for space, light, nutrients and water) and stochastic events (mortality and fires) determine the state of vegetation, response times to environmental perturbations, and the successional development. In spite of this, state-of-art reconstructions of past transient vegetation changes have not been accounted for in landscape evolution models. Here, a widely used dynamic vegetation model (LPJ-GUESS) was used to simulate vegetation composition/ cover and surface runoff in Chile for the Last Glacial Maximum (LGM), Mid Holocene (MH) and present day (PD). In addition, we conducted transient vegetation

25 simulations from LGM to PD for four sites of the Coastal Cordillera of Chile at a spatial and temporal resolution adequate for coupling with landscape evolution models.

Using a regionally-adapted parametrization, LPJ-GUESS was capable of reproducing present day potential natural vegetation along the strong climatic gradients of Chile and simulated vegetation cover was also in line with satellite-based observations. Simulated vegetation during the LGM differed markedly from PD conditions. Coastal cold temperate

30 rainforests where displaced northward by about 5° and the tree line and vegetation zones were at lower elevations than at PD. Transient vegetation simulations indicate a marked shift in vegetation composition starting with the past-glacial warming that coincides with a rise in $[CO_2]$. Vegetation cover between the sites ranged from 13% (LGM: 8%) to 81% (LGM: 73%) for the northern Pan de Azúcar and southern Nahuelbuta sites, respectively, but did not vary by more than 10% over the 21,000 yr simulation. A sensitivity study suggests that $[CO_2]$ is an important driver of vegetation changes and,

35 thereby, potentially landscape evolution. Comparisons with other paleoclimate model driver highlight the importance of model input on simulated vegetation.

In the near future, we will directly couple LPJ-GUESS to a landscape evolution model (see companion paper) to build a fully-coupled dynamic-vegetation/ landscape evolution model that is forced with paleoclimate data from atmospheric general circulation models.

40

1. Introduction

On the macro scale, it has been suggested that sediment yields from rivers exhibit a non-linear relationship with changing vegetation (Langbein and Schumm, 1958). Although this relationship is controversial (e.g. Riebe et al., 2001; Gyssels et al., 2005), previous work highlights that vegetation is likely a first order control on catchment denudation rates (Acosta et al.,
5 2015; Collins et al., 2004; Istanbulluoglu and Bras, 2005; Jeffery et al., 2014). While relatively simple vegetation descriptions have been included in landscape evolution modelling studies (Collins et al., 2004; Istanbulluoglu and Bras, 2005), these descriptions do not include explicit representations of plant competition for water, light and nutrients or stand dynamics which are key to determine the progression of vegetation state.

Dynamics Global Vegetation Models (DGVMs) were created as state-of-art tools for representing the distribution of
10 vegetation types, vegetation dynamics (forest succession and disturbances by, e.g., fire), vegetation structure and biogeochemical exchanges of carbon water and other elements between the soil, the vegetation and the atmosphere (Prentice et al., 2007). Interactions with the climate system have been a special focus, including both transient response to climatic changes and using DGVMs as land-surface schemes of Earth system models (i.e. Cramer et al., 2001; Bonan, 2008; Reick et al., 2013; Yu et al., 2016). DGVMs are instrumental for understanding the impact of future climate change on vegetation (i.e.
15 Morales et al., 2007; Hickler et al., 2012) as well as studying feedbacks between changing vegetation on climate (i.e. Raddatz et al., 2007; Brovkin et al., 2009). In addition, DGVMs have been utilised to better understand past vegetation changes, ranging from the Eocene (Liakka et al., 2014; Shellito and Sloan, 2006) and Late Miocene (Forrest et al., 2015) to the Last Glacial Maximum (LGM; ~21,000 BP) to the Mid Holocene (MH, ~6,000 BP) (i.e. Harrison and Prentice, 2003; Allen et al., 2010; Prentice et al., 2011; Huntley et al., 2013). Using these models, it has been shown that vegetation often
20 responds with substantial time lags to changes in climate (Hickler et al., 2012, Huntley et al., 2013). Such transient changes are likely to influence erosion rates and catchment denudation.

Past vegetation changes are however not only the results of changes in climate. The atmospheric CO_2 concentration [CO_2] has varied substantially through Earth's history (i.e. Brook 2008) and is an important limiting factor of photosynthesis and plant growth (Hickler et al., 2015). Glacial [CO_2] of approx. 180 ppm is close to the CO_2 compensation point of about 120
25 ppm for C_3 plants, implying that the majority of all plants on Earth were severely CO_2-limited in the LGM relative to today. Vegetation models tend to overestimate the cover of forest during the last glacial if they do not account for the strong limiting effect of [CO_2] (Harrison and Prentice, 2003). Furthermore, changes in [CO_2] also affect stomatal conductance and, thereby, plant water stress, plant productivity, and the hydrological cycle (Gerten et al., 2005). Although the magnitude of so-called "CO_2 fertilization effects" is still highly debated (Hickler et al., 2015), physiological effects of [CO_2] might be an
30 important driver of landscape evolution.

While DGVMs are in principle very widely applicable, simulations setups do require modification and calibration for particular applications. For regional applications, DGVMs should be tested against present-day data in the study region and process representations should be adapted to specific conditions (Hickler et al., 2012, Seiler et al., 2014). Climate data for simulations of paleovegetation often originates from Global Climate Models (GCMs), which have a rather coarse grid cell
35 resolution. Hence, spatial downscaling is necessary to derive climatic drivers at an adequate scale.

This study is part of the German EarthShape priority research program (www.earthshape.net), which investigates how biota shapes Earth surface processes along the climatic gradient in the Coastal Cordillera of Chile. Here, we describe the climate data processing and vegetation modelling approach, and report results of simulations for the last 21,000 years (part 1). Specifically, we developed a) a regionally-adapted setup of LPJ-GUESS that also includes improvements in sub-grid
40 representation of vegetation (required for future coupling), b) simulated potential natural vegetation (PNV) for Chile for present day (PD), MH and LGM climate conditions, and c) conducted transient simulations for four focus sites (Fig. 1) in monthly resolution spanning the full period from LGM to PD. Furthermore, we d) investigate the effect of [CO_2] and the use of different paleoclimate data for vegetation simulations of the LGM, and e) explore the relationship between vegetation

state, vegetation cover and simulated surface runoff. A companion paper (part 2, Schmid et al., this issue) presents a sensitivity analysis of how transient climate and vegetation impact catchment denudation. This component is evaluated through implementation of transient vegetation effects for hillslopes and rivers in a landscape evolution model. Although the approaches presented in these two companion papers are not fully coupled, the results of predicted vegetation cover change

5 derived by our vegetation simulations provide the basis for magnitudes of change in vegetation cover implemented in the companion paper. Together - these two papers provide a conceptual basis for understanding how transient climate and vegetation could impact catchment denudation. As a follow-up to the two presented studies we plan to couple the vegetation and landscape evolution models.

2. Background

10 ### 2.1. Climate of Chile

The location of Chile at the Pacific Ocean, its vast meridional extent of 4,345 km, and its steep topographic longitudinal profile result in highly variable climatic conditions. Large-scale subsidence of air masses over the southeast Pacific Ocean and other regional factors (e.g. relative cold coastal ocean currents) yield extremely arid deserts conditions in northern Chile with as little as 2-20 mm of annual precipitation (Garreaud and Aceituno, 2007). In the south, a 1000 km long narrow band

15 of Mediterranean-type climate exists at the western side of the Andes (Armesto et al., 2007). According to a general bioclimatic classification by Amigo and Ramírez (1998), the tropical/ Mediterranean boundary is located at 24° S (coast) to 27° S (inland) and the Mediterranean/ temperate boundary at 36-37° S while the temperate/ boreal boundary traverses from 52° S to 53.5° S. The Mediterranean-type climate is dominated by winter rain and hot dry summers of two to six months (Donoso, 1996). To the south, mid-latitude westerly winds and orographic uplift by the coastal mountains and Andes give

20 rise to annual precipitation amounts of up to 3000 mm and 5000 mm, respectively (Veblen et al., 1996). El Niño occurrences generally lead to above-average precipitation rates in the austral winter and spring in the Mediterranean zone and reduced precipitation at 38° S to 41° S in the following austral summer (Garreaud and Aceituno, 2007; Montecinos and Aceituno, 2003).

2.2. Vegetation of Chile

25 While virtually no vegetation can survive in the hyper-arid desert zone, approximately 12,000 km^2 of the Atacama Desert region are covered by perennial plants in the coastal ranges (*lomas*). Vegetation cover increases at lower altitudes in the presence of fog, or to the South with increasing precipitation (Rundel et al., 2007). Sclerophyllous woodlands and forests extend from 31° S to 37.5° S (Fig. 1; pictures depict the landscapes of focus sites discussed in this manuscript) and range from xeric thorn savanna elements to dense herbaceous cover in the Central Depression to sclerophyllous forests at

30 intermediate elevations. These vegetation types transition into the temperate deciduous *Nothofagus* forests (*Maule* or *Nothofagus* parklands, dominant species: *Nothofagus obliqua*, *N. glauca* and *N. alessandrii*) at the costal ranges and the lower Andes ranges before forming a broader vegetation zone (Donoso, 1982; Villagrán, 1995). With increasingly hydric conditions evergreen broadleaved species begin to dominate forest stands at approximately 40° S and form the Valdivian rainforest (the northernmost rainforest type, ranging from 37°45' S to 43°20' S) with high biomass and arboreal biodiversity

35 and evergreen, deciduous and needleleaved species (Veblen 2007). Further south the less diverse North Patagonian rainforest is mainly dominated by *N. betuloide* (Veblen 2007) and transitions into the Magellanic rainforest at approx. 47.5° S and Magellanic moorland with water-logged soils and poor nutrition status at the coast (Arroyo et al., 2005). Cold deciduous forests stretch from 35° S to 55° S along the Andes, covering cooler and dryer sites as compared to the coastal rainforests. These forests occur at altitudes of approx. 1300 m and gradually descend to sea level in Tierra del Fuego (Pollmann, 2005).

In Tierra del Fuego and east of the low Andes in southern Patagonia a gramineous steppe exists (Moreira-Muñoz, 2011), and high-Andean steppe also extends north at higher altitudes.

3. Methods

3.1. Vegetation model

5 The Lund-Potsdam-Jena General Ecosystem Simulator (LPJ-GUESS; Smith et al., 2001, 2014) is a state-of-the-art dynamic vegetation model that also simulates detailed stand dynamics using a gap-model approach (Bugmann, 2001; Hickler et al., 2004). The model is developed by an international community of scientists and has been used in more than 200 peer-reviewed international publications, including model evaluations against a large variety of benchmarks including vegetation type distribution, vegetation structure and productivity, as well as carbon and water cycling, at regional to global scales

10 (http://www.nateko.lu.se/lpj-guess). Vegetation development and functioning is based on the explicit simulation of photosynthesis rates, stomatal conductance, phenology, allometric calculations, and carbon and nutrient allocation. The model simulates growth and competition of different plant functional types (PFT, see Bonan et al., 2002) based on their competition for space, water, nutrients and light. Population dynamics are then simulated as stochastic processes that are influenced by current resource status, life-history and demography for each PFT. To enable a representative description of

15 average site conditions within a landscape each grid cell is simulated as a number of replicate patches in order to allow different (stochastic) disturbance histories and development (successional) stages (see Hickler et al., 2004; Wramneby et al., 2008). Fire occurrence is determined by the model using temperature, fuel load and soil moisture levels (Thonicke et al., 2001). Soil hydrology in LPJ-GUESS is represented by a simple two-layer bucket model with percolation between layers and deep drainage (see Gerten et al., 2004).

20 Vegetated surface area and runoff are affected by a range of model parameters in LPJ-GUESS. In 'cohort'-mode, an average individual of each PFT with a given age and development status is used to characterise vegetation state. Depending on PFT-specific parameters (i.e. maximum crown area, sapling density, allometric properties, leaf-to-sapwood area), age and competition for light, water, space, nutrients and demographic processes (establishment and mortality) individual cohorts can develop different states.

25 We approximate the land surface covered by vegetation with foliar projected cover (FPC) - the vertical projection of leaf area onto the ground (see Wramneby et al., 2010). In LPJ-GUESS it is derived from daily leaf area index (LAI, leaf area to ground area ratio, $m^2\ m^{-2}$) summed for all simulated PFTs using Lambert-Beer extinction law (originally proposed by Monsi and Saeki in 1953 for estimation of light extinction in plant canopies, see translation in Monsi and Saeki, 2005; Prentice et al., 1993).

$$A[\%] = \left(1.0 - \exp\left(-0.5 * \sum_{i=0}^{n} PFT_{LAI}\right)\right) * 100$$

(1)

Thus, depending on the composition of PFTs and the disturbance regime varying levels of ground cover can be simulated that not only reflect the environmental conditions, but also vegetation diversity and development.

35 In addition, the hydrological cycle is also affected by PFT-specific interception and transpiration rates that are a function of PFT specific parameters and development stage and thus vegetation is modulating infiltration and runoff under the given environmental constraints. Total runoff in LPJ-GUESS is calculated as the excess of water over field capacity of the upper soil layer (surface runoff), the lower soil layer (subsurface runoff), and the percolation rate through the second layer

(baseflow) (see Gerten et al., 2004 for details). The model does neither consider lateral water movement between grid cells nor routing in a stream network (in this study we report the surface runoff component only, see Gerten et al., 2004).

3.2. Landform classification

To bridge the gap in spatial resolution between LPJ-GUESS (typical spatial resolution of 0.5°x0.5°) and the landscape evolution model LandLab (Hobley et al., 2017; Schmid et al., this issue, typical spatial resolution ~100 m) and so facilitate future coupling of these models, we introduced the concept of landform disaggregation of grid cell conditions to smaller sub-pixel entities (Fig. 2). The advantages of introducing sub-pixel entities as opposed to simply performing higher resolution simulations are twofold. Firstly, higher-resolution simulations require climate forcing data of the desired output resolution that are not available for the intended simulation periods and region (and are not generally available for past time periods). Secondly, using sub-pixel entities incurs smaller additional computation costs than higher resolution simulations.

Sub-pixel entities, hereafter termed 'landforms', were derived for each grid cell using SRTM1-based elevation models (Kobrick and Crippen, 2017). Pixels from the elevation model (30 m spatial resolution) were classified based on their elevation (200 m bands) and their association with topographic features (ridges, mid-slope positions, valleys, and plains - based on slope and aspect) and similar pixels were grouped to form the landforms. The elevation of the landforms was used for temperature modification using an assumed lapse rate of 6.5 °C km^{-1} (relative to the default 0.5°x0.5° grid cell elevation and temperature). The slope and aspect were utilized to adjust the incoming radiation received by the landform. The general topographic features were used to modify the depth of the lower soil layer (deeper soils at valleys and plains, shallow soils at ridges) and to identify areas (valleys and plains) with a newly implemented time-buffered deep-water storage pool only accessible by tree PFTs. The classification resulted in 2 to 56 (mean: 17) landforms for each grid cell depending on topographic complexity.

In the proposed future coupled model, we envisage that the landform classification will be performed using elevation information from the landscape evolution model. The resulting per-landform (but non-spatially explicit) vegetation simulation results will be matched back to spatially explicit grid cells in the landscape evolution model, thus bridging the scale gap between the two models.

In the simulations presented here, all classified landforms with an area >1 % of the total land area in a grid cell were simulated using 15 replicate patches each, and simulation results were aggregated by area-weighting the results to the grid cell level. Biome classifications were carried out at the landform level and the grid cell biome classification was derived by aggregating landform results using a largest-area-based resampling.

3.3. Parametrization of plant functional types and biome classification

In a previous study Escobar Avaria (2013) implemented a first regional simulation for Chilean ecosystems (also using LPJ-GUESS) for present day (PD) climate conditions using a region-specific parametrization, which the presented study adapts and builds upon. Eleven PFTs - three shrub types, seven tree types and one herbaceous type - were defined in order to describe the major vegetation communities of Chile (Table B1). The definition of these PFTs are generally based on the proposed macro-units of Chilean vegetation (Luebert and Pliscoff, 2006) and follow the concept of representative/ or dominant species for describing a physiognomic unit. Apart from growth habit and associated traits, PFTs were designed to differentiate between leaf morphology and strategy, shade-tolerant and shade-intolerant varieties, their adaption to water access (mesic, xeric type), and root distribution. An overview of major eco-zones, associated PFTs and representative species is given in Table 1.

Using a biomization approach (see Prentice and Guiot, 1996 for the general concept), we classified the simulated PFTs into discrete vegetation types (referred to as biomes in the manuscript, see Fig. B1 for details of the classification procedure). Based on LAI thresholds and the ratio of certain key PFTs or PFT groups (i.e. boreal tree PFTs, xeric PFTs) to their peers, a

cascading decision tree was implemented that leads to eleven biomes resembling the general vegetation zones of Chile (Fig. 1), but also includes additional biome classes to capture the finer nuances of transitions between semi-arid and mesic vegetation communities and open woodlands (biomes are highlighted with *italic* in the text). To keep the number of vegetation types reasonable we designed multiple decision paths for biomes that exist as dense forest ecosystems but also

5 transition into lower canopy woodlands or transition into more open woodlands (i.e. *Magellanic Forest*, *Cold Deciduous Forest*; see Fig. B1). The classification was conducted at the landform level after the simulated 15 patches were averaged and the grid cell classification was derived from picking the area-dominant class of the landforms of a grid cell.

3.4. Environmental driving data and modelling protocol

The climate forcing data for LPJ-GUESS is derived from TraCE-21ka (Liu et al., 2009), which is a transient coupled

10 atmosphere-ocean simulation from LGM to PD using the Community Climate System Model version 3 (CCSM3; Collins et al., 2006). In this study we present time-slice simulations for the LGM, MH and PD (1960-1989), using perpetual climate forcing data from 30-year monthly climatologies (Fig. 3). In addition, we show results from a transient model simulation that utilises the full time-series data from the LGM to PD. All simulations were preceded by a 500-year spin-up period with de-trended climate data until vegetation and soils reached steady-state. For time-slice simulations the last 30 years of the

15 simulation were used.

Monthly temperature, precipitation, and downward shortwave radiation from the TraCE-21ka dataset (resolution T31; ~3.7°) were downscaled to 0.5°x0.5° spatial resolution and bias-corrected using a monthly climatology from the ERA-Interim reanalysis (Dee et al., 2011, years 1979-2014). The number of rain days within each month (used by LPJ-GUESS to distribute monthly precipitation totals to daily time steps internally) was derived from the monthly mean precipitation in the

20 TraCE-21ka data and the day-to-day precipitation variability from ERA-Interim (see Appendix A). [CO_2] for each simulation year was obtained from Monnin et al. (2001) and Meinshausen et al. (2017). A comparison climate dataset for the LGM (referred to as ECHAM5 in the manuscript) was provided by Mutz et al. (2017). Soil texture data used for bare-ground initialization of the model was obtained from the ISRIC-WISE soil dataset (Batjes, 2012) and a default soil depth of 1.5 m (0.5 m topsoil, 1 m subsoil) was assumed.

25 We simulated vegetation dynamics using the process-based dynamic vegetation model LPJ-GUESS (Smith et al., 2001) version 3.1 (Smith et al., 2014) with the model additions outlined above. The model runs were carried out without nitrogen limitation, using the CENTURY carbon cycle model (see Smith et al., 2014). Patch destroying disturbance and establishment intervals were defined as 100 and 5 years, respectively, and fire dynamics were enabled. Further details of the PFT specific parametrizations are given in Table B1. The transient site-scale model runs were conducted for the four focus sites of the

30 EarthShape SPP only due to i) computing resource constraints, ii) comparability with other EarthShape SPP work (see Schmid et al., this issue), and iii) better interpretability.

4. Results

In this study we present results for two types of simulations. First, we show results for time-slice (LGM, MH, PD) simulations. Direct model results (simulated LAI of individual PFTs) are presented first (Sect. 4.1) and then aggregated to a

35 biome representation for easier visualisation and comparison (Sect. 4.2). Then, foliar projected cover and surface runoff are investigated (Sect. 4.3). Second, we present results from the transient LGM-to-PD site simulations (Sect. 4.4).

4.1. Distribution of simulated plant functional types

Vegetation communities (expressed as assemblages of PFTs in LPJ-GUESS) establish spatially depending on a) environmental controls, b) competition, and c) stochastic events (i.e. fire incidents and mortality). An overview of the

simulated vegetation distribution expressed as the simulated LAI for each PFT under PD climate conditions is given in Fig. 4 (for key PFT properties see Table B1, the PFT distribution maps for LGM and MH are given in the supplemental material as Fig. S1 and Fig. S2 for completeness). Temperate broadleaved evergreen trees (TeBE$_{tm}$, TeBE$_{itm}$; t = shade-tolerant, it = shade-intolerant; m = mesic) dominate the coastal and central areas between latitudes 40° S to 46° S but also extend north

5   into the Mediterranean zone. Further to the north, temperate broadleaved summergreen PFTs (TeBS$_{tm}$, TeBS$_{itm}$) occur, with the shade-tolerant type dominating a relative small area between 37° S and 40° S. Northward, and at coastal areas, the sclerophyllous temperate evergreen PFT (TeBE$_{itscl}$; scl = sclerophyllous) starts to dominate, and with dryer conditions the total LAI (LAI$_{tot}$) is dominated by evergreen and raingreen shrubs (TeE$_s$, TeR$_s$; s = shrub). South of 40° S and, on higher terrain also further north, boreal broadleaved summergreen and evergreen tree PFTs (BBS$_{itm}$, BBE$_{itm}$) as well as boreal

10   evergreen shrubs (BE$_s$) establish. On the Andean ranges, and, to a lesser extent also as secondary components in the lowlands and coastal ranges from 35° S to 50° S, temperate needleleaved evergreen trees (TeNE) are simulated. Herbaceous vegetation (C3G) dominates LAI$_{tot}$ at high altitudes along the Andean ranges and is also a substantial contributor to total LAI in the Mediterranean zone (30° S to 38° S). To a lesser extent it contributes in most other regions but the hyper-arid desert. LAI$_{tot}$ is highest in the zone 36° S to 50° S. While LAI decreases substantially at sea level towards the Atacama Desert,

15   higher values of LAI extend further north at higher altitudes (see inset in Fig. 4).

4.2. Distribution of simulated biomes at LGM, MH and present

The simulated biome distribution changes spatially (Fig. 5a), vertically (Fig. 5b) and over time. Under PD climate, the simulated Valdivian temperate rainforests extend from 38° S to 46° S at the coast and transitions into the *Magellanic Forests/ Woodlands*, that are dominated by the boreal PFTs. A small zone of *Deciduous 'Maule' Forest* occurs to the north

20   of the *Valdivian Rainforest* as total rainfall decreases and rainfall seasonality increases. With even dryer conditions the *Sclerophyllous Woodland* type establishes, and as the fraction of trees and LAI$_{tot}$ is reduced even further with increasing temperatures and even lower annual rainfall, eventually give way to shrub dominated *Matorral* and finally the *Arid Shrubland* type. The *Cold Deciduous Forest* type is classified for parts of Tierra del Fuego, and on higher elevations of the lower Andes in Patagonia. It also forms larger zones at altitude between 30° S and 40° S. *Mesic Woodland* occurs between

25   34° S and 30° S at altitude (above the *Sclerophyllous Woodland* zone dominating the lowlands) and high-Andean *Steppe* occurs between 18° S and 30° S. A cold desert is present above the tree line in Patagonia and the highest Andean ranges, whereas hot desert (LAI$_{tot}$ <0.2) is simulated for areas from 20° S to 26° S. Owing to the similarity in climatic conditions (Fig. 3), the distribution simulated for the MH does not differ substantially from PD (Table 2). The northern border of *Sclerophyllous Woodland* shifts to approximately 34° S, giving way to a *Matorral* zone. In addition, the *Cold Deciduous*

30   *Forest* biome covers larger areas in Patagonia at the expense of *Magellanic Woodland* (+27.5%; -9.1%; Table 2). The spatial and vertical distribution of biomes for the LGM is however markedly different (Fig. 5a,b). The substantially lower temperatures (Fig. 3) lead to an expansion of cold deserts up to 45° S (coastal areas) and 40° S (higher altitudes), respectively. The boreal PFT dominated *Magellanic Woodland* biome is substantially reduced in extend (16.5% (LGM) vs. 32.6% (PD) of simulated area, Table 2) and shifted further north (40° S to 45° S at the coast, 43° S to 35° S at higher

35   altitudes inland). The area covered by temperate rainforest is restricted to a small lowland area from 36° S to 40° S, and the larger areas of *Cold Deciduous Forest* at altitude are also substantially smaller (Fig. 5b; Table 2). Lowland *Steppe* and *Mesic Woodland* biomes are simulated instead of *Matorral* and *Sclerophyllous Woodlands* and desert covers larger areas of the high-Andes to the north.

4.3. Foliar projected cover and surface runoff

40   The percentage of ground covered, and thus shielded from strong denudation, and surface runoff (as a major driver of erosion rates) are both influenced by the composition and state of vegetation communities. We therefore evaluate the

regional and temporal changes of these important variables as simulated by LPJ-GUESS for the LGM, MH and PD time slices. The simulated LAI of PFTs can be aggregated and converted to foliar projected cover (see Eq. (1)) and thus allows us to estimate the surface covered by vegetation. It should however be noted that this is only an approximation of true ground cover as small-scale vegetation variations are not simulated location-specific (spatial lumping effects are not considered for

5 instance). However, the implementation of a sub-grid landform scale was, in part, motivated to improve the models' prediction of smaller scale differences as it should allow to differentiate different sub-grid conditions for the major landforms within one simulation cell. Low FPC clearly coincides with distribution of hyper- to semi-arid biomes (Fig. 5a, 6a). Under PD climate conditions, average FPC for the semi-arid and Mediterranean biome types *Arid Shrubland*, *Matorral*, and *Sclerophyllous Woodland* are 16%, 35%, and 66%, respectively (Table 3) and cover increases southward with increases

10 in annual precipitation rates (Fig. 3b). South of 35° S, FPC values >70% are simulated for most grid cells except for high-altitude locations, the glacier fields of North Patagonia, and parts of the Magellanic moorland at the coast (see also Table 3). A strong positive correlation between annual rainfall and FPC can be observed for all semi-arid, Mediterranean, and seasonally dry temperature eco zones (Fig. 7a) and increases in annual rainfall lead to a strong rise of ground covered until 250-300 mm rainfall per year (*Arid Shrubland*: +14.5–16.3% 100 mm^{-1}; *Matorral:* +12.9-16.5% 100 mm^{-1}; *Steppe*: +13.5-

15 17.8% 100 mm^{-1}; Fig. 7a). At these levels, Mediterranean and temperate woodland biomes start to dominate but increases in precipitation raise FPC only by +2.7-3.3% 100 mm^{-1} and +5.4-6.4% 100 mm^{-1} (*Sclerophyllous Woodland, Mesic Woodland*). Similar spatial pattern of FPC can be observed for the MH (Fig. 6a) and for the relationship to precipitation rates (Fig. 7a). No significant difference in FPC to PD conditions are apparent for the Atacama Desert and most temperate forest areas from 36° S to 42° S. FPC at high-Andes locations of the north and large parts of the *Magellanic Forest* and *Cold Deciduous*

20 *Forest* biomes in the south is 10-20% lower than under PD climate, whereas for the Mediterranean zone FPC was reduced by 5-10% (Fig. 6b, Table 3).

Due to lower temperatures and reduced precipitation rates at high altitudes and in the southern part of the country (Fig. 3), FPC at LGM in these areas is simulated to be strongly reduced (< -30%, cold desert conditions for large areas south of 46° S) but FPC was lower for all areas of Chile (Fig. 6b, Table 3). While the general correlation of FPC to precipitation can also

25 be observed for LGM (Fig. 7a), the variability in mesic and xeric woodlands appears to be larger.

Annual average runoff varies greatly from north to south (Fig. 6c) and is strongly correlated to annual precipitation (Fig. 3, 7b). For PD and MH climate, LPJ-GUESS simulated almost no surface runoff for arid and Mediterranean areas of Chile to approx. 32° S (see also Table3). Runoff rates increase gradually southward and reach their peak (> 2000mm yr^{-1}) in areas of hyper-humid conditions along the Pacific coast. MH runoff rates are higher for areas of the Northern Patagonian and

30 Magellanic rainforests (40° S – 46° S), but lower for coastal areas of the Magellanic moorlands (Fig. 6d). LGM runoff rates are higher for most areas (Table 3) and especially south of 34° S, with strongest differences occurring from 40° S to 46° S.

4.4. Transient changes of simulated vegetation from LGM to present

In this section we present transient simulation results for grid cells that contain the EarthShape focus sites (Fig. 8). The results presented in this section are given for a single landform of the simulated grid cells in order to preserve successional

35 transitions between PFTs might would otherwise be lost through averaging. The field site location and the represented area of the chosen landform within the grid cell are marked in the insets of Fig. 8a-d.

Temperatures and [CO_2] start to increase at 18,000 BP and a marked pull-back in temperatures during the Antarctic Cold Reversal (~14,500 BP) is present in the TraCE-21ka data for all four sites (Fig. 8a-d). Annual precipitation at the site Pan de Azúcar (21.11° S 70.55° W, 320 m a.s.l.) is extremely low (38-40 mm, hyper-arid) for the entire simulation period (Fig. 8a).

40 Annual average temperature for the presented landform increases from 13.9 °C (LGM) to 16.8 °C (PD). As a result of these arid conditions only evergreen and raingreen shrubs and herbaceous vegetation can establish, and LAI, and consequently FPC, remains very low (LAI$_{tot}$ <0.3). For most episodes of the simulation this location is classified as desert according to the

implemented biomization scheme, with only two periods switching to another state (*Arid Shrubland*, LAI$_{tot}$ >0.2) at approx. 17,000 to 15,000 BP, and more permanently, the late Holocene. Fire return intervals (expressed as number of years between fire incidents) fluctuate greatly as fuel production is substantially limited by low vegetation growth. No surface runoff is simulated and FPC ranges from 8% (LGM) to 13% (PD).

5   Climatic conditions for site Santa Gracia (29.75° S 71.16° W, 579 m a.s.l.) show a similar temporal progression from LGM to PD, but average temperatures are lower and range from 11.9 °C (LGM) to 14.9 °C (PD) (Fig. 8b). Annual precipitation does not change substantially from LGM to PD (152 vs. 122 mm). Vegetation from LGM to approx. 18,000 BP is dominated by herbaceous vegetation, but (raingreen) shrubs increase with rising temperatures, leading to a biome shift from *Steppe* to *Matorral*. Fire return intervals decrease with increased (arboral) litter production due to encroachment of shrubs but FPC

10   only increases by 7% from 33% (LGM) to 40% (PD). Simulated surface runoff is insignificant for most simulation years.

Temperatures at the La Campana site (32.93° S 71.09° W, 412 m a.s.l.) increase from 11.0 °C (LGM) to 14.0 °C (PD), but annual precipitation amounts decrease from 446 mm (LGM) to approx. 320 mm slightly increasing again to 355 mm at PD. The simulated LGM vegetation for site La Campana is dominated by herbaceous vegetation and small fractions of temperate evergreen deciduous trees mixed with small fractions of boreal shrubs leading to a steppe biome classification with short

15   episodes of mesic woodlands (Fig. 8c). With the decrease of annual precipitation and increasing temperatures (approx. 17,500 BP) *Sclerophyllous Woodlands* displace the deciduous trees and evergreen and raingreen shrubs start to appear. The fire-return intervals shorten in this phase and reach values of less than 15 years for the remaining simulation. Raingreen shrubs expand at approx. 12,000 BP and push back on herbaceous vegetation and, in part, evergreen shrubs. The LAI of sclerophyllous broadleaved evergreen trees and shrubs increases further during the last 5,000 simulation years, which leads

20   to a shift in our biome classification from *Matorral* (LAI$_{tot}$ >0.5) to *Sclerophyllous Woodland* (LAI$_{woody}$ >1). Despite pronounced changes in vegetation composition, FPC only increases from approx. 51% (LGM) to 59% (PD).

Climatic conditions at the site Nahuelbuta (37.81° S 73.01° W, 1234 m a.s.l.) are markedly different from the three previous ones, as this location receives substantially higher annual precipitation throughout the time-series (> 1200 mm) and average temperatures at this latitude and elevation are substantially lower (5.1 °C for LGM and 8.6 °C for PD, Fig. 8d). Note

25   however, that the landform is only representative for a small fraction of the 0.5°x0.5° grid cell as it is located on mountainous terrain, whereas most areas in the cell are covered by coastal lowlands with higher annual temperatures and thus the site simulation results presented here differ from the total grid cell results presented in previous sections (see marked landform cover in inset, Fig 8d). LPJ-GUESS simulates a diverse composition of PFTs and a transition from boreal, *Magellanic Woodland* conditions at LGM, to a period of *Cold Deciduous Forest* (17,500 - 12,000 BP), followed by 12,000

30   years of *Valdivian Rainforest* and *Mesic Woodland* alternations. During the LGM, boreal broadleaved evergreen, deciduous tree and shrub PFTs dominate and form a forest. Annual precipitation (>1300 mm) and surface runoff (>440 mm) is high during that period. With rising temperatures, the boreal shrubs and evergreen tree PFTs are displaced by temperate needleleaved evergreen trees (TeNE) and increases in herbaceous vegetation. Temperate evergreen PFTs establish approx. 17,000 BP and, after another retreat at approx. 14,500 BP (coinciding with the Antarctic Cold Reversal), start to dominate

35   the forest at this location. Fire frequency is low for the first 4,000 simulation years and only rises to approx. one fire in 100 years afterwards. FPC remains at constantly high values (>75%) indicating a largely closed forest for the entire simulation period.

5. Discussion

The aim of this study was to demonstrate that a dynamic vegetation model with suitable modifications can simulate the state

40   and transient changes of vegetation structure and composition at a temporal and spatial resolution that enables coupling with landscape evolution models. To bridge the spatial scales as is necessary for such a coupling, we included sub-gridcell

landform types in the DGVM to provide finer scale vegetation cover information which can be provided to a landscape evolution model. Using this modified model with present day climate data and a regional parameterisation of Chilean vegetation produced a good description of the present day vegetation of Chile (Fig. 1, 4, 5, 9; details in Sect. 5.1 below). Temporal compatibility was demonstrated by paleovegetation simulations which showed reasonable agreement with past

5 vegetation states and transitions as has been reconstructed by proxy data (discussed in Section 5.2 below). The results also indicate that the simulated vegetation is strongly influenced by climatic model drivers (see Sect. 5.3) and $[CO_2]$ (see Sect. 5.4), and by feedback mechanism occurring within the model (i.e. fire return intervals as controlled by climate and the production of fuel). Given the sensitivity of the vegetation cover to the climate forcing, careful consideration must be made of paleoclimate data and its characteristics and uncertainties. The TraCE-21ka data does not show high levels of variability,

10 instead exhibiting only gradual changes over time (temperature, $[CO_2]$) or no strong, centennial to millennial scale trends (precipitation). In contrast, available proxy data suggest stronger variability, at least locally, although this is difficult to generalize for larger areas (see Sect. 5.2). Regional paleoclimate simulations with higher spatial resolution might be required to obtain better landscape-scale model forcing. Another approach could be to modify the climate-model-derived forcing based on proxy-data, such as increasing inter- and intra-annual variability within reasonable ranges (e.g. Giesecke et al.,

15 2010).

LPJ-GUESS explicitly simulates the soil moisture available for vegetation through a simple hydrological cycle (Gerten et al., 2004), and it is thus possible to assess changes in runoff due to changes in transpiration, evaporation and percolation. Such information, in particular surface runoff, may also be provided to a landscape evolution model in a coupled model configuration. The surface run-off simulated here was found to be consistent with expected patterns. However, it should be

20 noted that the model uses a simple two-layer bucket model which cannot truly represent catchment scale hydrological features (i.e. no lateral flow, routing, or variable water table) but has been successfully coupled to mechanistic hydrological models (Pappas et al., 2015).

5.1. Evaluation of model predicted PNV

The model was able to simulate the general distribution of biomes of Chile for most regions (Fig. 5), but accuracy for the

25 occurrence of deciduous PFTs was low (*Deciduous 'Maule' Forest*, *Cold Deciduous Forest*, also previously reported by Escobar Avaria, 2013). The simulated vegetation cover was slightly lower than satellite-based estimates by MODIS Vegetation Continuous Field product (Townshend, 2017), likely due to differences in foliar projected cover and total satellite-observed vegetation cover, but the general patterns were represented (Fig. 9). Most distinct regional discrepancy can be observed at coastal areas between 30° S to 36° S, which might be attributed to the lack of fog-precipitation in our model.

30 Fog precipitation is strongly dependent on distance to the coast, local topography, wind fields, and stratification of the troposphere (Lehnert et al., 2018) and can potentially contribute significant amounts of precipitation (Garreaud et al., 2008). However, a model representation in LPJ-GUESS is difficult due to the scale mismatch and a lack of required input variables to determine the occurrence of fog. Second, precipitation amounts in the model drivers might be too low as the coarse spatial resolution of the original input data may lead to an underrepresentation of orographic precipitation effects (i.e. Leung and

35 Ghan, 1998). It also has to be noted that the MODIS VCF product was found to overestimate cover in sparsely vegetated areas (Sexton et al., 2013) and thus should rather be treated as a general guideline. Lastly, LPJ-GUESS was applied to simulate the PNV whereas MODIS VCF observes actual vegetation that includes anthropogenic land-use (agricultural fields, degradation due to grazing, etc.).

5.2. Comparison to vegetation change proxy data

40 While regional vegetation cover of the past is difficult to quantify, there are limited site-scale pollen, lake level, and midden proxy datasets available to evaluate model behaviour for past climate conditions in Chile (Marchant et al., 2009).

Pollen data from rodent midden (Quebrada del Chaco, 25.5° S, 2670-3550 m, Maldonado et al., 2005) suggest higher winter precipitation at the LGM, higher annual precipitation at 17-14 ka BP and higher summer precipitation at 14-11 ka BP in northern Chile, but results from another study at lower elevations indicate absolute desert conditions throughout the quaternary (Diaz et al., 2012) - which could be caused by regional to fog-precipitation. TraCE-21ka precipitation for site Pan

5   de Azúcar (located at similar latitudes but at coastal lowlands) does not vary from PD conditions throughout the time series and as a result LPJ-GUESS simulates very little vegetation cover (Fig. 8a). Other studies also suggest that LGM conditions were extremely dry, but that the transition to modern climatic conditions in this area occurred as a non-linear process of multiple moisture pulses over several centuries (Grosjean et al., 2001). Pollen reconstructions from Laguna de Tagua Tagua 34.5° S 71.16° W (Heusser, 1990; Valero-Garcés et al., 2005) indicate the presence of extensive temperate woodlands at the

10   LGM that match the simulated *Mesic Woodland* biome for this location in our simulations (Fig. 4a). Multiple lake sediment records of the region indicate dry and warm conditions at MH and the onset of more humid, but strongly seasonal, conditions (winter rainfall) in the late Holocene (Heusser, 1990; Villa-Martínez et al., 2003; Valero-Garcés et al., 2005). While LPJ-GUESS does simulate Mediterranean vegetation types (*Matorral* and *Sclerophyllous Woodland*) for the MH and a shift to denser xeric woodlands in the late Holocene for this region, substantial variations in the precipitation regime as suggested by

15   the lake records are not present in the TraCE-21ka data used.

Pollen records from the Chilean Lake District show a warming trend starting at 17,780 BP (Moreno and Videla, 2016), followed by a trend reversal with major cooling events (14,500 and 12,700 BP). In TraCE-21ka, a sharp cooling event at 14,500 is present (likely as an effect of the simulation setup of Meltwater Pulse 1A, Liu et al., 2009), but the second event is not. In our transient simulations this event is reflected in changes of vegetation composition at three out of our four sites.

20   This climatic change to colder and dryer conditions leads to a reduction of shrub PFTs at sites Sta. Gracia (Fig. 8b) and La Campana (Fig. 8c) that established with rising temperature and [CO_2] starting 18,000 BP. As a result, the site biome classification for Sta. Gracia briefly swings back to the initial *Steppe* state and the reduced fuel accumulation leads to fewer fires. Surface runoff is however not affected due to the low precipitation rates. In contrast, the same event at site La Campana does not result in changes of the fire frequency probably due to the presence of sufficient fuel due to higher annual

25   rainfall rates (>350 mm). At site Nahuelbuta this event briefly delays a transition from cold deciduous PFTs to a temperate evergreen/ needleleaved forest (Fig. 8d).

The early and mid-Holocene were the driest periods for central Chile (Heusser 1990; Valero-Garcés et al., 2005; Maldonado and Villagrán, 2016). This is also visible in the TraCE-21ka dataset (La Campana and Nahuelbuta, Fig 8c,d). However, the annual precipitation differences in the TraCE-21ka data of this period compared to LGM and PD are relatively minor and we

30   thus might not fully capture the true vegetation dynamics indicated by the proxy data of the region (centennial shifts from dry xeric to humid mesic vegetation).

Pollen proxy data by Villagrán (1988) indicates that coastal cool evergreen rainforests were shifted by 5° northwards during the LGM relative to their current position and that these areas were covered by forest mosaics/ parklands instead of todays' dense forest. LPJ-GUESS simulations for LGM do reproduce this latitudinal biome shift (Fig. 5a). While we could not

35   classify an open parkland vegetation type, the simulations show 5-20% lower FPC for this area at LGM (Fig. 6b) which can be interpreted as more open conditions. For the MH, temperate Valdivian rainforests similar to PD conditions did exist (Villagrán, 1988) and are also simulated by LPJ-GUESS (Fig. 5a)

LGM reductions of temperatures of up to 12 °C have been proposed for high altitudes in the tropics (Thompson et al., 1995), and LPJ-GUESS also simulates a more expansive belt of high-elevation cold desert for LGM at the expense of high-Andean

40   steppe (Fig. 5a,b). Furthermore, significantly lower tree lines and vegetation zones of up to 1500 m compared to PD are reported for LGM (Marchant et al., 2009), which in our simulations is reflected in smaller areas of the *Cold Deciduous Forest* biome and a shift to lower elevations (Fig. 5b).

In summary, the main forest transition in south-central Chile from LGM to PD was the postglacial expansion of forests (~15 ka BP). However, strong climate seasonality and forest clearing during early land utilization (as indicated by increased fire activities from 12–6 ka BP) and forest expansion into abandoned land after the Spanish colonial period (Lara et al., 2012) were other major, but anthropogenic, vegetation changes which were followed by intense land clearing for lumber extraction and farming (Armesto et al., 2010). Although significant for many areas, we opted to exclude anthropogenic land use in our analysis as spatial intensities and general utilization is not well understood and hard to qualify and as we see this beyond the scope of this study.

5.3. Sensitivity of simulation to paleoclimate input data

As demonstrated in this study, climatic forcing of the ecosystem model is crucial for the simulated vegetation composition, biome establishment and associated vegetation cover and surface runoff, which are key controls of catchment denudation rates (Jeffery et al., 2014). The TraCE-21ka dataset was chosen since, to our knowledge, it is the only available dataset providing continuous transient monthly data. The low spatial resolution (T31/ ~3.75°) is however problematic in resolving regional scale heterogeneity and we therefore compare our LGM simulations with a regional paleoclimate model simulation (ECHAM5, resolution: T159/ 0.75°x0.75°, Mutz et al., 2017). Although the general latitudinal patterns of temperature deviations from PD are similar to TraCE-21ka, precipitation gradients and regional anomalies at LGM are stronger (see Fig. 3 for LGM anomaly plot of TraCE-21ka data and Fig. S1a,b for ECHAM5). While LGM precipitation anomalies in TraCE-21ka do not exceed 650 mm, precipitation rates in the ECHAM5 data vary by well over 1500 mm for the Andean highlands at 27-35° S and the coastal areas from 36-53° S but are markedly lower for the lower Andes and Tierra del Fuego (Fig. S1b). This leads to a different pattern of biome distribution for the LGM (Fig. 10). Due to lower temperatures, the cold deserts extend further north and a small zone of temperate rainforest exists at latitudes 40° S to 42° S, whereas *Magellanic Woodlands* are simulated with TraCE-21ka. A zone classified as *Magellanic Woodland* stretches from 30° S to 42° S along the Andean range that gives way to *Cold Deciduous Forest* at 28° S to 32° S at altitude. Temperate *Deciduous "Maule" Forest* exists north of 40° S and transitions into *Sclerophyllous Woodland* extending to 30° S, whereas TraCE-21ka results lead to *Steppe* at the lowlands and *Mesic Woodlands* at higher altitudes. Higher precipitation levels north of 30° S also lead to higher vegetation cover and larger areas of *Matorral* and *Arid Shrubland* and a reduction of desert conditions. This results in substantial differences of simulated foliar projected cover (Fig. 10b). While cover of *Steppe* and *Mesic Woodlands* simulated with TraCE-21ka is generally 10-20% higher versus the ECHAM5 simulations, the cover from 35° S to the Atacama Desert is substantially lower than ECHAM5 (higher precipitation rates for this region). Cover south of 42° S is substantially higher for TraCE-21ka as the colder conditions in ECHAM5 simulations generally prohibit the vegetation establishment.

The results show that choice of paleoclimate data clearly has an influence on simulated vegetation composition, but the impact on vegetation cover depends on the type and location of change. For instance, forest-to-forest transitions due to changes in temperature can have only little effect on FPC, while a different rate of annual precipitation at Mediterranean to semi-arid conditions can lead to substantial changes of FPC (Sta. Gracia: +200-500 mm precipitation in ECHAM5 LGM data results in > +20% FPC; see also Fig. 7a).

5.4. Impact of atmospheric CO_2 on vegetation cover

The effectiveness of photosynthesis, and thus the plants ability to build-up biomass, has a large dependence on $[CO_2]$ (Hickler et al., 2015; Zhu et al., 2016). Increases in vegetation biomass (expressed in LAI) were observed in our simulations but coincide with simultaneous rise of temperatures and $[CO_2]$ (Fig. 8b-d). To assess the direct effect of changes in $[CO_2]$, we conducted a sensitivity simulation under LGM climate conditions. We compared the default LGM simulations (TraCE-21ka, $[CO_2]$ = ~180 ppm) with a pre-industrial $[CO_2]$ of 280 ppm (Fig. 11). This change leads to an expansion of vegetated

areas (high-Andean steppe), an increase of forest biomes at the expense of herbaceous vegetation (i.e., northward expansion of *Mesic Woodland*, *Cold Deciduous Forests*, and *Valdivian Rainforest* and the establishment of small pockets of *Sclerophyllous Woodland*) (Fig. 11a). In all vegetated areas FPC increases with higher $[CO_2]$, most notably between 30-40° S (+ 5-10% FPC). Such changes and the magnitude of the CO_2 effect are consistent with earlier LGM simulations (Harrison

5   and Prentice, 2003). They suggest that $[CO_2]$ could have a crucial role also for understanding landscape evolution. The strong limiting role of $[CO_2]$ during the LGM is generally accepted, but to what extent substantial CO_2 fertilization effects still occur as concentrations increase to rise beyond the current stage is highly debated (Hickler et al., 2015). However, the LPJ-GUESS model with the enabled nitrogen cycle, and nitrogen limiting CO_2 effects, has been shown to generally reproduce experimental observations from "Free Air CO2 Enrichment" (FACE) experiments (e.g. Zaehle et al., 2014;

10 Medlyn et at al., 2015; De Kauwe et al., 2017). Enabling the nitrogen cycle in LPJ-GUESS would be crucial if one aims at understanding vegetation response and landscape evolution at $[CO_2]$ above present-day levels as it occurred in various episodes of Earths' history (i.e. the Miocene).

6. Conclusions

In this study, we demonstrated how a DGVM can be applied to estimate vegetation features through time that can play an

15 important role for evolution of landforms, and at a spatial and temporal resolution adequate for coupling with landscape evolution models. The simulation also captures vegetation change drivers that are not included in simplified vegetation representations used so far in landscape evolution models, such as plant-physiological effects of $[CO_2]$. The sensitivity of landscape evolution to vegetation and climate changes is evaluated in the companion paper by Schmid et al. (this issue). Although our two studies stop short of presenting results from a fully coupled (dynamic vegetation and surface process)

20 models, the results we present highlight a) how much vegetation likely changed in the Coastal Cordillera of Chile since the LGM (this study), and b) the general sensitivity of topography and erosion rates to the magnitudes of change identified here (Schmid et al., this issue). Ongoing work will present the next step of fully coupled simulations. From the experiments presented here, our main conclusions are as follows:

(1)   The regionally adapted version of LPJ-GUESS was able to simulate the latitudinal and altitudinal distribution of
25   potential natural vegetation and the satellite-observed vegetation cover for present day conditions in most areas of Chile.

(2)   While simulated MH vegetation did not differ substantially compared to PD PNV, simulated vegetation of the LGM indicates a marked northward shift of the biome distribution, a reduction of the tree line, and downward shift of vegetation zones at altitude. Vegetation cover was generally reduced compared to PD conditions and cold and hot
30   desert were covering substantially larger areas of the simulation domain.

(3)   Analysis of the results from transient site simulation indicate that temperature and $[CO_2]$ did cause most of the observed shifts in vegetation composition and, in some cases, transitions between biomes over time. A sensitivity study highlighted the impact of 'CO2-fertilization' on vegetation cover under LGM climate conditions.

(4)   Comparisons with proxy data suggest that the coarse-scale climatic forcing does underestimate centennial to millennial
35   climate variability. A combination of proxy-derived estimates and climate model results or higher resolution climate models might be necessary to capture such variability.

(5)   Our results show that vegetation cover in semi-arid to Mediterranean ecosystems responds strongly to changes in precipitation, while change of climatic conditions for temperate to boreal forest ecosystems do so only to a lesser extent.

In summary, we suggest that coupling state-of-art dynamic vegetation modelling with landscape evolution models has great potential for improving our understanding of the evolution of landforms. The current simulations are an important step towards applying such a coupled model to the study area of EarthShape.

5 **Acknowledgements**

This study was funded as part of the German science foundation priority research program EarthShape: Earth surface shaping by biota (grant EH329-14-1 to T. A. E. and HI1538/5-1 to T. H.). We also thank the national park service of Chile (CONAF) for access to the study areas during field excursions.

10 **Competing interests**

The authors have no conflict of interest to declare.

References

Acosta, V. T., Schildgen, T. F., Clarke, B. A., Scherler, D., Bookhagen, B., Wittmann, H., von Blanckenburg, F., and
15   Strecker, M. R.: Effect of vegetation cover on millennial-scale landscape denudation rates in East Africa, Lithosphere, 7(4), 408–420, doi: 10.1130/L402.1, 2015.

Allen, J. R. M., Hickler, T., Singarayer, J. S., Sykes, M. T., Valdes, P. J., and Huntley, B.: Last glacial vegetation of northern Eurasia, Quat. Sci. Rev., 29, 2604-2618, doi: 10.1016/j.quascirev.2010.05.031, 2010.

Amigo, J. and Ramírez, C.: A bioclimatic classification of Chile: woodland communities in the temperate zone, Plant
20   Ecology, 136(1), 9–26, 1998.

Armesto, J. J., Manuschevich, D., Mora, A., Smith-Ramirez, C., Rozzi, R., Abarzua, A. M., and Marquet, P. A.: From the Holocene to the Anthropocene: A historical framework for land cover change in southwestern South America in the past 15,000 years, Land Use Policy, 27(2), 148–160, doi: 10.1016/j.landusepol.2009.07.006, 2010.

Armesto, J. J., Arroyo, M. T. K., and Hinojosa, L. F.: The Mediterranean environment of central Chile, in: The Physical
25   Geography of South America, edited by: Veblen, T. T., Young, K. R., and Orme, A. R., Oxford University Press, 184-199, 2007.

Arroyo, M. T. K., Pliscoff, P., Mihoc, M. and Arroyo-Karlin, M.: The Magellanic moorland, in: The World's Largest Wetlands, edited by: Fraser, L. H. and Keddy, P. A., Cambridge University Press 424–445, 2005.

Batjes, N. H.: ISRIC-WISE Derived soil properties on a 5 by 5 arc-minutes grid (version 1.2), ISRIC Report 2012/01, 2012.

30 Bonan, G. B.: Forests and climate change: Forcings, feedbacks, and the climate benefits of forests, Science, 320(5882), 1444–1449, doi: 10.1126/science.1155121, 2008.

Bonan, G. B., Levis, S., Kergoat, L., and Oleson, K. W.: Landscapes as patches of plant functional types: An integrating concept for climate and ecosystem models, Glob. Biogeochem. Cycles, 16(2), 1021–1025, doi: 10.1029/2000GB001360, 2002.

35 Brook, E.: Windows on the greenhouse, Nature, 453(7193), 291-292, 2008.

Brovkin, V., Raddatz, T., Reick, C. H., Claussen, M., and Gayler, V.: Global biogeophysical interactions between forest and climate, Geophys. Res. Lett., 36, L07405, doi: 10.1029/2009GL037543, 2009.

Bugmann, H.: A review of forest gap models, Climatic Change, 51(3/4), 259–305, 2001.

Collins, D. B. G., Bras, R. L., and Tucker, G. E.: Modeling the effects of vegetation-erosion coupling on landscape
40   evolution, J. Geophys. Res. Earth. Surf., 109(F3), F03004, doi: 10.1029/2003JF000028, 2004.

Collins, W. D., Bitz, C. M., Blackmon, M. L., Bonan, G. B., Bretherton, C. S., Carton, J. A., Chang, P., Doney, S. C., Hack, J., James, Henderson, T. B., Kiehl, J. T., Large, W. G., McKenna, D. S., Santer, B. D., and Smith, R. D.: The Community Climate System Model Version 3 (CCSM3), J. Clim., 19(11), 2122–2143, doi: 10.1175/JCLI3761.1, 2006.

Cramer, W., Bondeau, A., Woodward, F., Prentice, I., Betts, R., Brovkin, V. and, Cox, P., Fisher, V., Foley, J., Friend, A.,
5   Kucharik, C. and, Lomas, M., Ramankutty, N., Sitch, S., Smith, B, White, A., and Young-Molling, C.: Global response of terrestrial ecosystem structure and function to CO_2 and climate change: results from six dynamic global vegetation models, Glob. Change Biol., 7(4), 357–373, doi:10.1046/j.1365-2486.2001.00383.x, 2001.

Dai, A.: Precipitation characteristics in eighteen coupled climate models, J. Clim., 19(18), 4605–4630, doi: Precipitation Characteristics in Eighteen Coupled Climate Models, 2006.

10   Dee, D. P., Uppala, S. M., Simmons, A. J., Berrisford, P., Poli, P., Kobayashi, S., Andrae, U., Balmaseda, M. A., Balsamo, G., Bauer, P., Bechtold, P., Beljaars, A. C. M., Berg, L. van de, Bidlot, J., Bormann, N., Delsol, C., Dragani, R., Fuentes, M., Geer, A. J., Haimberger, L., Healy, S. B., Hersbach, H., Hólm, E. V., Isaksen, L., Kållberg, P., Köhler, M., Matricardi, M., McNally, A. P., Monge-Sanz, B. M., Morcrette, J. J., Park, B. K., Peubey, C., Rosnay, P. de, Tavolato, C., Thépaut, J. N., and Vitart, F.: The ERA-Interim reanalysis: configuration and performance of the data assimilation
15   system, Q. J. Royal Meteorol. Soc., 137(656), 553–597, doi: 10.1002/qj.828, 2011.

De Kauwe, M. G., Medlyn, B. E., Walker, A. P., Zaehle, S., Asao, S., Guenet, B., Harper, A. B., Hickler, T., Jain, A. K., Luo, Y., Lu, X., Luus, K., Parton, W. J., Shu, S., Wang, Y.-P., Werner, C., Xia, J., Pendall, E., Morgan, J. A., Ryan, E. M., Carrillo, Y., Dijkstra, F. A., Zelikova, T. J., Norby, R. J.: Challenging terrestrial biosphere models with data from the long-term multifactor Prairie Heating and CO_2 Enrichment experiment, Glob. Change Biol., 23, 3623–3645, doi:
20   10.1111/gcb.13643, 2017.

Diaz, F. P., Latorre, C., Maldonado, A., Quade, J. and Betancourt, J. L.: Rodent middens reveal episodic, long-distance plant colonizations across the hyperarid Atacama Desert over the last 34,000 years, J. Biogeogr., 39(3), 510–525, doi: 10.1111/j.1365-2699.2011.02617.x, 2012.

Donoso, C.: Ecology of *Nothofagus* forests in Central Chile, in: The ecology and biogeography of *Nothofagus* forests, edited
25   by: Veblen, T. T., Hill, R. S., and Read, J., Yale University Press., 271–292, 1996.

Donoso, C. D. O.: Reseña ecologica de los bosques mediterraneos de Chile, Bosque (Valdivia), 4(2), 117–146, 1982.

Escobar Avaria, C. A.: Simulating current regional pattern and composition of Chilean native forests using a dynamic ecosystem model, Student thesis series INES, http://lup.lub.lu.se/student-papers/record/3877156, 2013.

Forrest, M., Eronen, J. T., Utescher, T., Knorr, G., Stepanek, C., Lohmann, G., and Hickler, T.: Climate-vegetation
30   modelling and fossil plant data suggest low atmospheric CO_2 in the late Miocene, Clim. Past, 11(12), 1701–1732, doi: 10.5194/cp-11-1701-2015, 2015.

Garreaud, R. and Aceituno, P.: Atmospheric circulation and climatic variability, in: The Physical Geography of South America, edited by: Veblen, T. T., Young, K. R., and Orme, A. R., Oxford University Press, 45-59, 2007.

Garreaud, R., Barichivich, J., Christie, D. A., and Maldonado, A.: Interannual variability of the coastal fog at Fray Jorge
35   relict forests in semiarid Chile, J. Geophys. Res., 113(G4), doi: 10.1029/2008JG000709, 2008.

Gerten, D., Schaphoff, S., Haberlandt, U., Lucht, W., and Sitch, S.: Terrestrial vegetation and water balance - hydrological evaluation of a dynamic global vegetation model, J. Hydrol., 286(1-4), 249–270, doi: 10.1016/j.jhydrol.2003.09.029, 2004.

Gerten, D., Lucht, W., Schaphoff, S., Cramer, W., Hickler, T., and Wagner, W.: Hydrologic resilience of the terrestrial
40   biosphere, Geophys. Res. Lett., 32(21), L21408, doi: 10.1029/2005GL024247, 2005.

Giesecke T., Miller, P. A., Sykes M. T., Ojala, A. E. K., Seppä, H., and Bradshaw, R. H. W.: The effect of past changes in inter-annual temperature variability on tree distribution limits, J. Biogeogr., 37(7), 1394-1405, doi: 10.1111/j.1365-2699.2010.02296.x, 2010.

Grosjean, M., Van Leeuwen, J. F. N., Van Der Knaap, W. O., Geyh, M. A., Ammann, B., Tanner, W., Messerli, B., Núñez, L. A., Valero-Garcés, B. L., and Veit, H.: A 22,000 14C year BP sediment and pollen record of climate change from Laguna Miscanti (23°S), northern Chile, Glob. Planet. Change, 28(1-4), 35–51, doi: 10.1016/S0921-8181(00)00063-1, 2001.

5   Gyssels, G., Poesen, J., Bochet, E., and Li, Y.: Impact of plant roots on the resistance of soils to erosion by water: a review, Prog. Phys. Geogr., 29(2), 189–217, doi: 10.1191/0309133305pp443ra, 2005.

Harrison, S. P. and Prentice, C. I.: Climate and CO_2 controls on global vegetation distribution at the last glacial maximum: analysis based on palaeovegetation data, biome modelling and palaeoclimate simulations, Glob. Change Biol., 9(7), 983–1004, doi: 10.1046/j.1365-2486.2003.00640.x, 2003.

10   Heusser, C. J.: Ice age vegetation and climate of subtropical Chile, Palaeogeogr. Palaeoclimatol. Palaeoecol., 80(2), 107–127, 1990.

Hickler, T., Smith, B., Sykes, M. T., Davis, M. B., Sugita, S., and Walker, K.: Using a generalized vegetation model to simulate vegetation dynamics in northeastern USA, Ecology, 85(2), 519–530, doi: 10.1890/02-0344, 2004.

Hickler, T., Vohland, K., Feehan, J., Miller, P. A., Smith, B., Costa, L., Giesecke, T., Fronzek, S., Carter, T. R., Cramer, W.,
15   Kühn, I., and Sykes, M. T.: Projecting the future distribution of European potential natural vegetation zones with a generalized, tree species-based dynamic vegetation model, Glob. Ecol. Biogeogr., 21(1), 50–63, doi: 10.1111/j.1466-8238.2010.00613.x, 2012.

Hickler, T., Rammig, A. and Werner, C.: Modelling CO_2 impacts on forest productivity, Curr. Forestry Rep., 1(2), 1–12, doi: 10.1007/s40725-015-0014-8, 2015.

20   Hobley, D. E. J., Adams, J. M., Nudurupati, S. S., Hutton, E. W. H., Gasparini, N. M., Istanbulluoglu, E., and Tucker, G. E.: Creative computing with Landlab: an open-source toolkit for building, coupling, and exploring two-dimensional numerical models of Earth-surface dynamics, Earth Surf. Dyn., 5, 21–46, doi: 10.5194/esurf-5-21-2017, 2017.

Huntley, B., Allen, J. R. M., Collingham, Y. C., Hickler, T., Lister, A. M., Singarayer, J., Stuart, A. J., Sykes, M. T., and Valdes, P. J.: Millennial climatic fluctuations are key to the structure of Last Glacial ecosystems, PLOS One, 8(4),
25   e61963, doi: 10.1371/journal.pone.0061963, 2013.

Istanbulluoglu, E. and Bras, R. L.: Vegetation-modulated landscape evolution: Effects of vegetation on landscape processes, drainage density, and topography, J. Geophys. Res. Earth Surf., 110, F02012, doi: 10.1029/2004JF000249, 2005.

Jeffery, M. L., Yanites, B. J., Poulsen, C. J., and Ehlers, T. A.: Vegetation-precipitation controls on Central Andean topography, J. Geophys. Res. Earth Surf., 119(6), 1354–1375, doi: 10.1002/2013JF002919, 2014.

30   Kobrick, M. and Crippen, R.: SRTMGL1: NASA Shuttle Radar Topography Mission Global 1 arc second V003, doi: 10.5067/MEaSUREs/SRTM/SRTMGL1.003, 2017.

Langbein, W. B. and Schumm, S. A.: Yield of sediment in relation to mean annual precipitation, Transactions, American Geophysical Union, 39(6), 1076–1084, doi: 10.1029/TR039i006p01076, 1958.

Lehnert, L., Thies, B., Trachte, K., Achilles, S., Osses, P., Baumann, K., Schmidt, J., Samolov, E., Jung, P., Leinweber, P.,
35   Büdel, B., and Bendix, J.: A case study on fog/low stratus occurrence at Las Lomitas, Atacama Desert (Chile) as a water source for biological soil crusts, Aerosol Air Qual. Res., 18(1), 254-269, doi: Aerosol Air Qual. Res., 2018.

Leung, L. R. and Ghan, J., S.: Parameterizing subgrid orographic precipitation and surface cover in climate models, Mon. Weather Rev., 126(12), 3271–3291, doi: 10.1175/1520-0493(1998)126<3271:PSOPAS>2.0.CO;2, 1998.

Lara, A., Solari, M. E., Del Rosario Prieto, and Peña, M. P.: Reconstrucción de la cobertura de la vegetación y uso del suelo
40   hacia 1550 y sus cambios a 2007 en la ecorregión de los bosques valdivianos lluviosos de Chile (35° - 43° 30´ S). Bosque (Valdivia), 33(1), 03–04, doi: 10.4067/S0717-92002012000100002, 2012.

Liakka, J., Colleoni, F., Ahrens, B., and Hickler, T.: The impact of climate-vegetation interactions on the onset of the Antarctic ice sheet, Geophys. Res. Lett., 41(4), 1269–1276, doi: :10.1002/2013GL058994, 2014.

Liu, Z., Otto-Bliesner, B. L., He, F., Brady, E. C., Tomas, R., Clark, P. U., Carlson, A. E., Lynch-Stieglitz, J., Curry, W., Brook, E., Erickson, D., Jacob, R., Kutzbach, J., and Cheng, J.: Transient simulation of last deglaciation with a new mechanism for Bølling-Allerød warming., Science, 325(5938), 310–314, doi: 10.1126/science.1171041, 2009.

Luebert, F. and Pliscoff, P.: Sinopsis bioclimática y vegetacional de Chile, Editorial Universitaria, Santiago, Chile, 2006.

5 Maldonado, A., Betancourt, J. L., Latorre, C., and Villagran, C.: Pollen analyses from a 50 000-yr rodent midden series in the southern Atacama Desert (25° 30' S), J. Quat. Sci., 20(5), 493–507, doi: 10.1002/jqs.936, 2005.

Maldonado, A., and Villagrán, C.: Climate variability over the last 9900 cal yr BP from a swamp forest pollen record along the semiarid coast of Chile, Quaternary Research, 66(2), 246-258, doi: 10.1016/j.yqres.2006.04.003, 2006

Marchant, R., Cleef, A., Harrison, S. P., Hooghiemstra, H., Markgraf, V., Boxel, J. van, Ager, T., Almeida, L., Anderson, R.,
10 Baied, C., Behling, H., Berrio, J. C., Burbridge, R., Bj orck, S., Byrne, R., Bush, M., Duivenvoorden, J., Flenley, J., De Oliveira, P., Geel, B. van, Graf, K., Gosling, W. D., Harbele, S., Hammen, T. van der, Hansen, B., Horn, S., Kuhry, P., Ledru, M. P., Mayle, F., Leyden, B., Lozano-Garc 'ıa, S., Melief, A. M., Moreno, P., Moar, N. T., Prieto, A., Reenen, G. van, Salgado-Labouriau, M., Sch abitz, F., Schreve-Brinkman, E. J., and Wille, M.: Pollen-based biome reconstructions for Latin America at 0, 6000 and 18 000 radiocarbon years ago, Clim. Past, 5(4), 725–767, doi:
15 10.5194/cp-5-725-2009, 2009.

Medlyn, B. E., Zaehle, S., De Kauwe, M. G., Walker, A. P., Dietze, M. C., Hanson, P. J., Hickler, T., Jain, A. K., Luo, Y., Parton, W., Prentice, I. C., Thornton, P. E., Wang, S., Wang, Y.-P., Weng, E., Iversen, C. M., McCarthy, H. R., Warren, J. M., Oren, R., and Norby, R. J.: Using ecosystem experiments to improve vegetation models. Nat. Clim. Change 5, 528–534, doi:10.1038/nclimate2621, 2015.

20 Meinshausen, M., Vogel, E., Nauels, A., Lorbacher, K., Meinshausen, N., Etheridge, D. M., Fraser, P. J., Montzka, S. A., Rayner, P. J., Trudinger, C. M., Krummel, P. B., Beyerle, U., Canadell, J. G., Daniel, J. S., Enting, I. G., Law, R. M., Lunder, C. R., O'Doherty, S., Prinn, R. G., Reimann, S., Rubino, M., Velders, G. J. M., Vollmer, M. K., Wang, R. H. J., and Weiss, R.: Historical greenhouse gas concentrations for climate modelling (CMIP6), Geosci. Model Dev., 10(5), 2057–2116, doi: 10.5194/gmd-10-2057-2017, 2017.

25 Monnin, E., Indermuhle, A., Dallenbach, A., Fluckiger, J., Stauffer, B., Stocker, T. F., Raynaud, D., and Barnola, J. M.: Atmospheric CO_2 concentrations over the last glacial termination, Science, 291(5501), 112–114, doi: 10.1126/science.291.5501.112, 2001.

Monsi, M. and Saeki, T.: On the factor light in plant communities and its importance for matter production, Ann. Bot., 95(3), 549–567, doi: 10.1093/aob/mci052, 2005.

30 Montecinos, A. and Aceituno, P.: Seasonality of the ENSO-related rainfall variability in central Chile and associated circulation anomalies, J. Clim., 16(2), 281–296, doi: 10.1175/1520-0442(2003)016<0281:SOTERR>2.0.CO;2, 2003.

Morales, P., Hickler, T., Rowell, D. P., Smith, B., and Sykes, M. T.: Changes in European ecosystem productivity and carbon balance driven by regional climate model output, Glob. Change Biol., 13(1), 108-122, doi: 10.1111/j.1365-2486.2006.01289.x, 2007.

35 Moreira-Muñoz, A.: Plant Geography of Chile, Springer Netherlands, Dordrecht., 2011.

Moreno, P., L. Jacobson, G., V. Lowell, T. and H. Denton, G.: Interhemispheric climate links revealed from a Late-glacial cool episode in southern Chile, Nature, 409, 804-808, doi: 10.1038/35057252, 2001.

Moreno, P. I. and Videla, J.: Centennial and millennial-scale hydroclimate changes in northwestern Patagonia since 16,000 yr BP, Quat. Sci. Rev., 149, 326-337, doi: 10.1016/j.quascirev.2016.08.008, 2016.

40 Mutz, S. G., Ehlers, T. A., Werner, M., Lohmann, G., Stepanek, C., and Li, J.: Where is Late Cenozoic climate change most likely to impact denudation?, Earth Surf. Dynam. Discuss., 1–37, doi: 10.5194/esurf-2017-47, 2017.

Pappas, C., Fatichi, S., Rimkus, S., Burlando, P. and Huber, M. O.: The role of local-scale heterogeneities in terrestrial ecosystem modeling, J. Geophys. Res. Biogeosci., 120, 341–360, doi:10.1002/2014JG002735, 2015.

Pollmann, W.: A long-term record of *Nothofagus* dominance in the southern Andes, Chile, Austral Ecol., 30(1), 91–102, doi: 10.1046/j.1442-9993.2004.01427.x 2005.

Prentice, I. C. and Guiot, J.: Reconstructing biomes from palaeoecological data: a general method and its application to European pollen data at 0 and 6 ka, Clim. Dyn., 12(3), 185–194, doi: 10.1007/BF00211617, 1996.

5 Prentice, I. C., Sykes, M. T., and Cramer, W.: A simulation model for the transient effects of climate change on forest landscapes, Ecol. Modell., 65(1-2), 51–70, doi: 10.1016/0304-3800(93)90126-D, 1993.

Prentice, I. C., Bondeau, A., Cramer, W., Harrison, S. P., Hickler, T., Lucht, W., Sitch, S., Smith, B., and Sykes, M. T.: Dynamic global vegetation modeling: Quantifying terrestrial ecosystem responses to large-scale environmental change Terrestrial Ecosystems in a Changing World, in: Terrestrial Ecosystems in a Changing World, edited by: Canadell, J.

10 G., Pataki, D. E., Pitelka, L. F., Springer, 175–192, 2007.

Prentice, I. C., Harrison, S. P., and Bartlein, P. J.: Global vegetation and terrestrial carbon cycle changes after the last ice age, New Phyt., 189(4), 988–998, doi: 10.1111/j.1469-8137.2010.03620.x, 2011.

Raddatz, T. J., Reick, C. H., Knorr, W., Kattge, J., Roeckner, E., Schnur, R., Schnitzler, K.-G., Wetzel, P. and Jungclaus, J.: Will the tropical land biosphere dominate the climate–carbon cycle feedback during the twenty-first century?, Clim.

15 Dync., 29(6), 565–574, doi: 10.1007/s00382-007-0247-8, 2007.

Reick, C. H., Raddatz, T., Brovkin, V., and Gayler, V.: Representation of natural and anthropogenic land cover change in MPI-ESM, J. Adv. Model. Earth Syst., 5(3), 459–482, doi: 10.1002/jame.20022, 2013.

Riebe, C. S., Kirchner, J. W., Granger, D. E., and Finkel, R. C.: Minimal climatic control on erosion rates in the Sierra Nevada, California, Geology, 29(5), 447–450, doi: 10.1130/0091-7613(2001)029<0447:MCCOER>2.0.CO;2, 2001.

20 Rundel, P. W., Villagra, P. E., Dillon, M. O., Roig-Juñent, S., and Debandi, G.: Arid and semi-arid ecosystems, in: The Physical Geography of South America, edited by: Veblen, T. T., Young, K. R., and Orme, A. R., Oxford University Press., 158-183, 2007.

Schmid, M., Ehlers, T. A., Werner, C., and Hickler, T.: Effect of changing vegetation on denudation (part 2): Landscape response to transient climate and vegetation cover, Earth Surf. Dyn. Discuss., 2018.

25 Seiler, C., Hutjes, R. W. A., Kruijt, B., Quispe, J., Añez, S., Arora, V. K., Melton, J. R., Hickler, T., and Kabat, P.: Modeling forest dynamics along climate gradients in Bolivia, J. Geophys. Res. Biogeosc., 119, 758–775, doi: 1002/2013JG002509, 2014.

Sexton, J. O., Song, X.-P., Feng, M., Noojipady, P., Anand, A., Huang, C., Kim, D.-H., Collins, K. M., Channan, S., DiMiceli, C., and Townshend, J. R.: Global, 30-m resolution continuous fields of tree cover: Landsat-based rescaling of

30 MODIS vegetation continuous fields with lidar-based estimates of error, , Int. J. Digit. Earth, 6(5), 427–448, doi: 10.1080/17538947.2013.786146, 2013.

Shellito, C. J. and Sloan, L. C.: Reconstructing a lost Eocene paradise: Part I. Simulating the change in global floral distribution at the initial Eocene thermal maximum, Glob. Planet. Change, 50(1), 1–17, doi: 10.1016/j.gloplacha.2005.08.001, 2006.

35 Smith, B., Prentice, I. C., and Sykes, M. T.: Representation of vegetation dynamics in the modelling of terrestrial ecosystems: comparing two contrasting approaches within European climate space, Global Ecol. Biogeogr., 10(6), 621–637, doi: 10.1046/j.1466-822X.2001.t01-1-00256.x, 2001.

Smith, B., Wårlind, D., Arneth, A., Hickler, T., Leadley, P., Siltberg, J., and Zaehle, S.: Implications of incorporating N cycling and N limitations on primary production in an individual-based dynamic vegetation model, Biogeosciences,

40 11(7), 2027–2054, doi: 10.5194/bg-11-2027-2014, 2014.

Thompson, L. G., Mosley-Thompson, E., Davis, M. E., Lin, P. N., Henderson, K. A., Cole-Dai, J., Bolzan, J. F., and Liu, K.-b.: Late Glacial Stage and Holocene tropical ice core records from Huascarán, Peru, Science, 269(5220), 46, doi: 10.1126/science.269.5220.46, 1995.

Thonicke, K., Venevsky, S., Sitch, S., and Cramer, W.: The role of fire disturbance for global vegetation dynamics: coupling fire into a Dynamic Global Vegetation Model, Glob. Ecol. Biogeogr., 10(6), 661–677, doi: 10.1046/j.1466-822X.2001.00175.x, 2001.

Townshend, J. R. G.: MOD44B: MODIS/Terra Vegetation Continuous Fields Yearly L3 Global 250m SIN Grid V006, doi: 10.5067/MODIS/MOD44B.006, 2017.

Valero-Garcés, B. L., Jenny, B., Rondanelli, M., Delgado-Huertas, A., Burns, S. J., Veit, H., and Moreno, A.: Palaeohydrology of Laguna de Tagua Tagua (34° 30′ S) and moisture fluctuations in Central Chile for the last 46 000 yr, J. Quat. Sci., 20(7-8), 625-641, doi: 10.1002/jqs.988, 2005.

Veblen, T. T., Donoso, C., Kitzberger, T. and Rebertus, A. J.: Ecology of southern Chilean and Argentinean *Nothofagus* forests, in: The ecology and biogeography of *Nothofagus* forests, edited by: Veblen, T. T., Hill, R. S., and Read, J., Yale University Press, 293–253, 1996.

Veblen, T. T.: Temperate forests of the Southern Andean region, in: The Physical Geography of South America, edited by: Veblen, T. T., Young, K. R., and Orme, A. R., Oxford University Press, 217-231, 2007.

Villa-Martínez, R., Villagran, C. and Jenny, B.: The last 7500 cal yr B.P. of westerly rainfall in Central Chile inferred from a high-resolution pollen record from Laguna Aculeo (34°S), Quat. Res., 60(3), 284–293, doi: 10.1016/j.yqres.2003.07.007, 2003.

Villagrán, C. M.: Expansion of Magellanic Moorland during the late Pleistocene: Palynological evidence from northern Isla de Chiloé, Chile, Quat. Res., 30(3), 304–314, doi: doi.org/10.1016/0033-5894(88)90006-3,1988.

Villagrán, C. M.: Quaternary history of the Mediterranean vegetation of Chile, in: Ecology and biogeography of Mediterranean ecosystems in Chile, California, and Australia, edited by: Arroyo, M. T. K., Zedler, P. H., Fox, M. D., Springer New York, 1995.

Wramneby, A., Smith, B., Zaehle, S., and Sykes, M. T.: Parameter uncertainties in the modelling of vegetation dynamics - Effects on tree community structure and ecosystem functioning in European forest biomes, Ecol. Modell., 216(3-4), 277–290, doi: 10.1016/j.ecolmodel.2008.04.013, 2008.

Wramneby, A., Smith, B., and Samuelsson, P.: Hot spots of vegetation-climate feedbacks under future greenhouse forcing in Europe, J. Geophys. Res., 115(D21), D21119, doi: 10.1029/2010JD014307, 2010.

Yu, M., Wang, G., and Chen, H.: Quantifying the impacts of land surface schemes and dynamic vegetation on the model dependency of projected changes in surface energy and water budgets, J. Adv. Model. Earth Syst., 8, 370–386, doi:10.1002/ 2015MS000492, 2016.

Zaehle, S., Medlyn, B. E., De Kauwe, M. G., Walker, A. P., Dietze, M. C., Hickler, T., Luo, Y., Wang, Y.-P., El-Masri, B., Thornton, P., Jain, A., Wang, S., Wårlind, D., Weng, E., Parton, W., Iversen, C. M., Gallet-Budynek, A., McCarthy, H., Finzi, A., Hanson, P. J., Prentice, I. C., Oren, R., and Norby, R. J.,: Evaluation of 11 terrestrial carbon-nitrogen cycle models against observations from two temperate Free-Air CO2Enrichment studies, New Phyt., 202, 803–822, doi: 10.1111/nph.12697, 2014.

Zhu, Z., Piao, S., Myneni, R. B., Huang, M., Zeng, Z., Canadell, J. G., Ciais, P., Sitch, S., Friedlingstein, P., Arneth, A., Cao, C., Cheng, L., Kato, E., Koven, C., Li, Y., Lian, X., Liu, Y., Liu, R., Mao, J., Pan, Y., Peng, S., Peñuelas, J., Poulter, B., Pugh, T. A. M., Stocker, B. D., Viovy, N., Wang, X., Wang, Y., Xiao, Z., Yang, H., Zaehle, S., and Zeng, N.: Greening of the Earth and its drivers, Nat. Clim. Change, 6, 791–795, doi: 10.1038/nclimate3004, 2016.

Table 1. Major vegetation zones, associated plant functional types (PFT), and representative species (modified after Escobar Avaria, 2013).

Biome	Plant functional type	Species
Arid Shrubland, Matorral, Sclerophyllous Woodland	Temperate evergreen shrubs (TeE$_s$) Temperate raingreen shrubs (TeR$_s$) Temperate broadleaved evergreen sclerophyllous trees (TeBE$_{itscl}$)	*Trevoa trinervis, Colliguaja odorifera, Quillaja saponaria, Lithraea caustica, Peumus boldus, Acacia caven, Prosopis spp*
Temperate 'Maule' Forest	Temperate summergreen deciduous trees (TeBS$_{tm}$, TeBS$_{itm}$)	*Nothofagus glauca, N. obliqua, N. alessandrii*
Valdivian Rainforest (incl. North Patagonian Rainforest)	Temperate broadleaved evergreen trees (TeBE$_{tm}$, TeBE$_{itm}$) Temperate needleaved evergreen trees (TeNE)	*Embothrium coccineum, Weinmannia trichosperma, N. dombeyi N. nitida, Eucryphia cordifolia, Drimys winteri Laureliopsis philippiana, Aextoxicon punctatum, Luma apiculata, Persea lingue, Amomyrtus luma Fitzroya cuppressoides, Pilgerodendron uviferum Saxegothaea conspicua, Podocarpus nubigena*
Magellanic Rainforest/ woodlands	Boreal broadleaved evergreen trees (BBE)	*N. betuloides*
Cold Deciduous Forest/ woodlands	Boreal broadleaved summergreen trees (BBS)	*N. pumilio, N. antarctica*
(not dominant) (High-Andean) Steppe	Boreal evergreen shrub (BE$_s$) Herbaceous vegetation (C3G)	-

Table 2. Areal extent of biomes in the simulation domain [units: percent of total area].

	LGM	MH	PD
Desert	53.7	12.6	7.6
Arid Shrubland	1.9	4.5	5.6
Matorral	1.2	3.9	2.3
Steppe	13.6	11.6	12.4
Sclerophyllous Woodland	-	5.6	8.7
Deciduous 'Maule' Forest	0.4	2.1	2.1
Mixed Forest	0.4	0.4	0.6
Valdivian Rainforest	4.1	11.2	13.4
Mesic Woodland	6.6	2.9	2.7
Cold Deciduous Forest	1.7	15.3	12
Magellanic Forest/ Woodland	16.5	29.8	32.6

Table 3. Average foliar projected cover (FPC) and annual surface runoff for simulated biomes at present day (PD) and relative change within these PD areas for Last Glacial Maximum (Δ LGM, LGM-PD) and Mid Holocene (Δ MH, MH-PD).

	Foliar projected cover [% cover]			Surface runoff [mm yr^{-1}]		
	PD	Δ LGM	Δ MH	PD	Δ LGM	Δ MH
Arid Shrubland	16	-5	-2	0	0	0
Matorral	35	-9	-5	0	0	0
Steppe	39	-23	-7	1	+4	+1
Sclerophyllous Woodland	66	-6	-4	187	+35	+9
Deciduous 'Maule' Forest	85	-5	0	638	+114	+33
Mixed Forest	85	-42	-1	193	+24	+5
Valdivian Rainforest	88	-20	-1	910	+93	+63
Mesic Woodland	56	-21	-10	81	+57	+10
Cold Deciduous Forest	78	-44	-6	200	+62	+13
Magellanic Forest/ Woodland	77	-68	-7	966	+124	+35

Figures
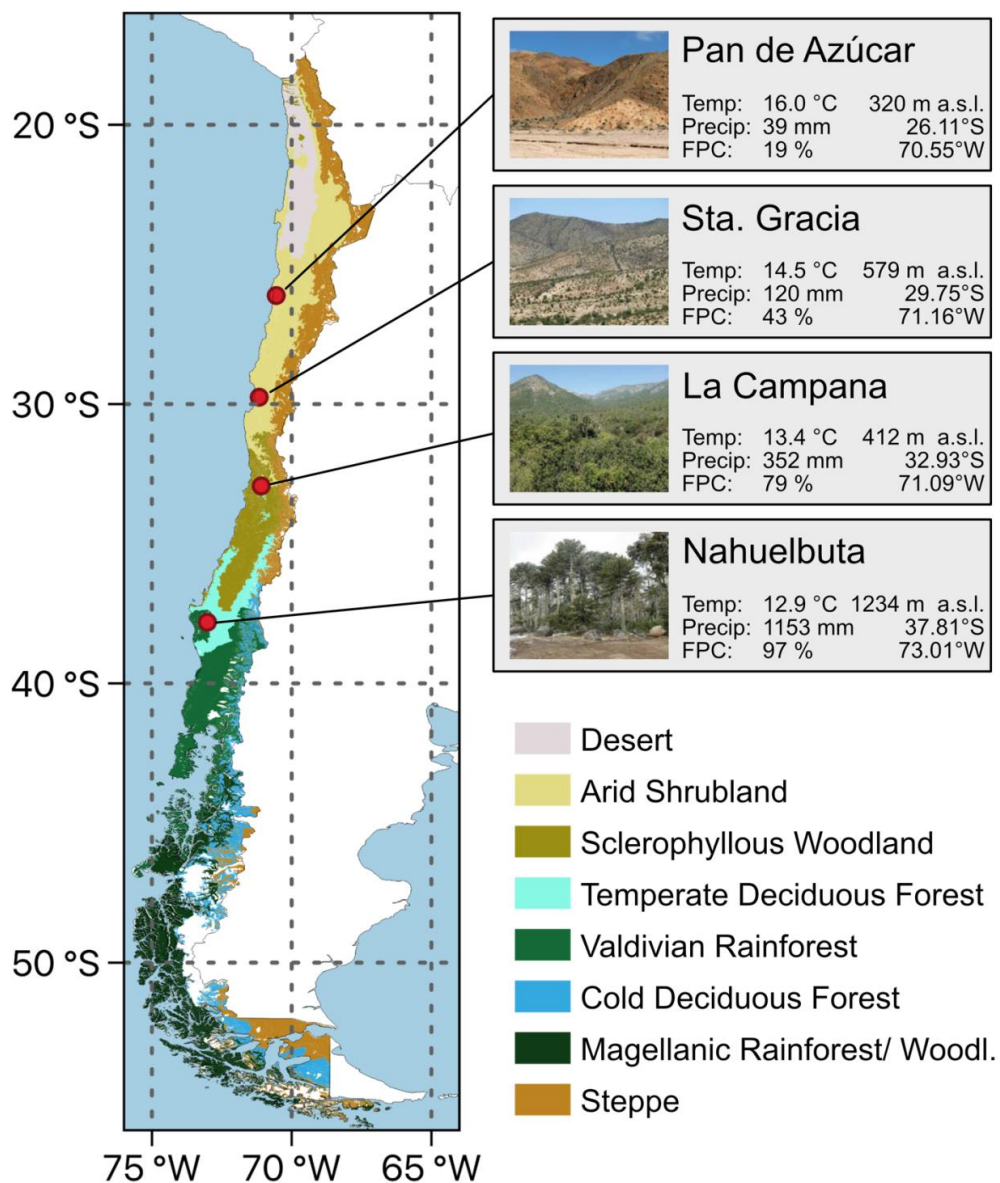
Figure 1. Distribution of major vegetation zones in Chile and location of the four EarthShape SPP focus sites Pan de Azúcar,

5   Sta. Gracia, La Campana and Nahuelbuta (temp: average annual temperature, precipitation: average annual precipitation -
data: ERA-Interim 1960-1989, FPC: foliage projected cover (MODIS VCF v6, total vegetation cover, 2001-2016 average,
Townshend, 2017). Vegetation zones are based on Luebert and Pliscoff (2006).
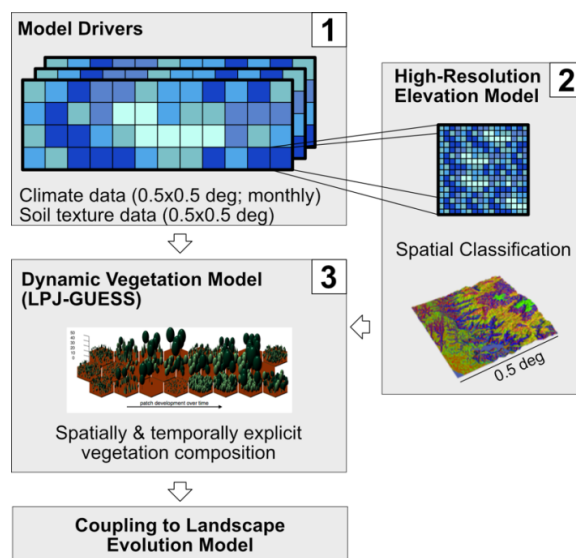
Figure 2. Schematic procedure of simulations. Coarse resolution model driving data (1) is disaggregated using a high-resolution elevation model and topographic landform classification (2) and the ecosystem model LPJ-GUESS then simulates vegetation state and dynamics using the landform classification to simulated topographic-adjusted patch composition (3).

5 Vegetation cover and surface runoff results can then be passed on to a coupled landscape evolution (LE) model (not implemented in presented study, see Schmid et al. in this issue for a description of the LE model).
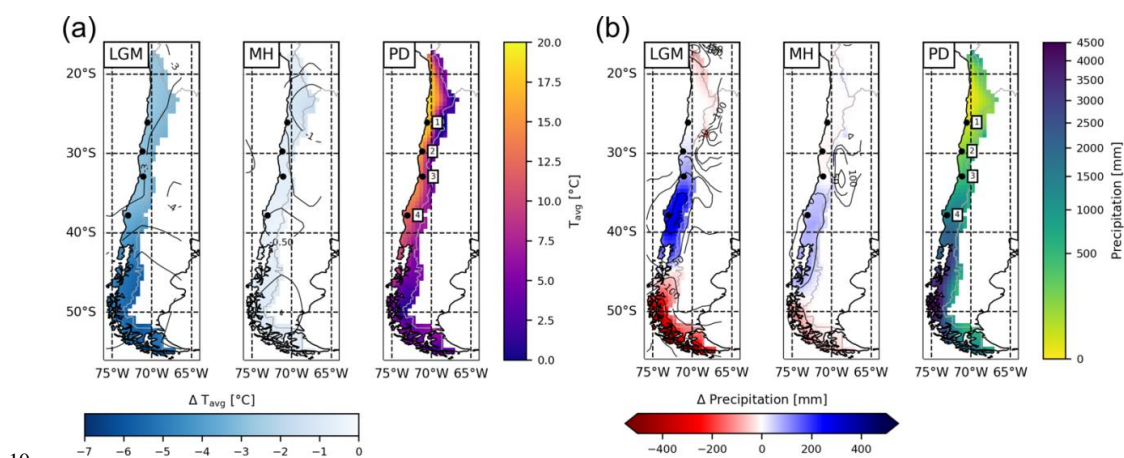
Figure 3. (a) Average annual temperature and **(b)** precipitation derived from the downscaled and bias-corrected TraCE-21ka transient paleoclimate data (Liu et al., 2009) for the Last Glacial Maximum (LGM), Mid Holocene (MH) and present day (PD) time-slices (data: average of 30-yr monthly data; 1: Pan de Azúcar, 2: Sta. Gracia, 3: La Campana, 4: Nahuelbuta).
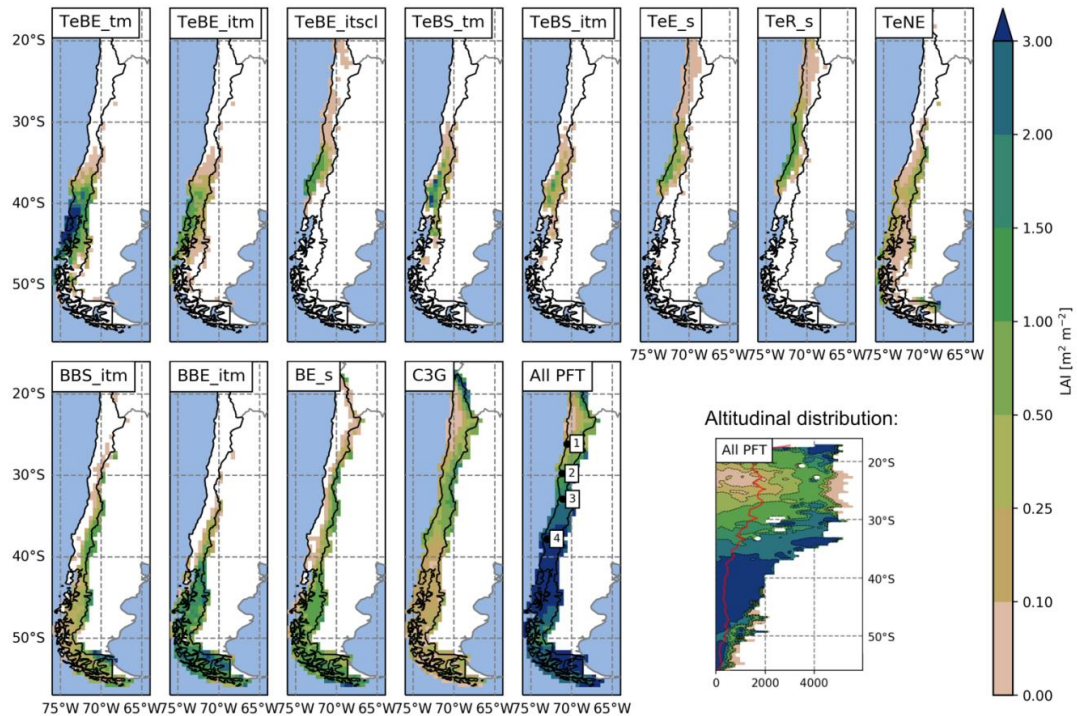
Figure 4. Spatial and altitudinal distribution of modelled plant functional types (PFT) for present day climate conditions (LAI: leaf area index [m^2 m^{-2}], the altitudinal subplot represents zonal mean LAI; red line: average elevation). PFTs: TeBE$_{tm}$/ TeBE$_{itm}$ (temperate broadleaved evergreen trees; t = shade-tolerant; it = shade-intolerant; m = mesic), TeBE$_{itscl}$ (temperate broadleaved evergreen trees; scl = sclerophyllous), TeBS$_{im}$/ TeBS$_{itm}$ (temperate broadleaved summergreen trees), TeE$_s$ (temperate evergreen shrubs; s = shrub), TeR$_s$ (temperate raingreen shrubs), TeNE (temperate needleleaved evergreen trees), BBS$_{itm}$ (boreal broadleaved summergreen trees), BBE$_{itm}$: (boreal broadleaved evergreen trees), BE$_s$: (boreal evergreen shrubs), C3G (herbaceous vegetation). 1: Pan de Azúcar, 2: Sta. Gracia, 3: La Campana, 4: Nahuelbuta.
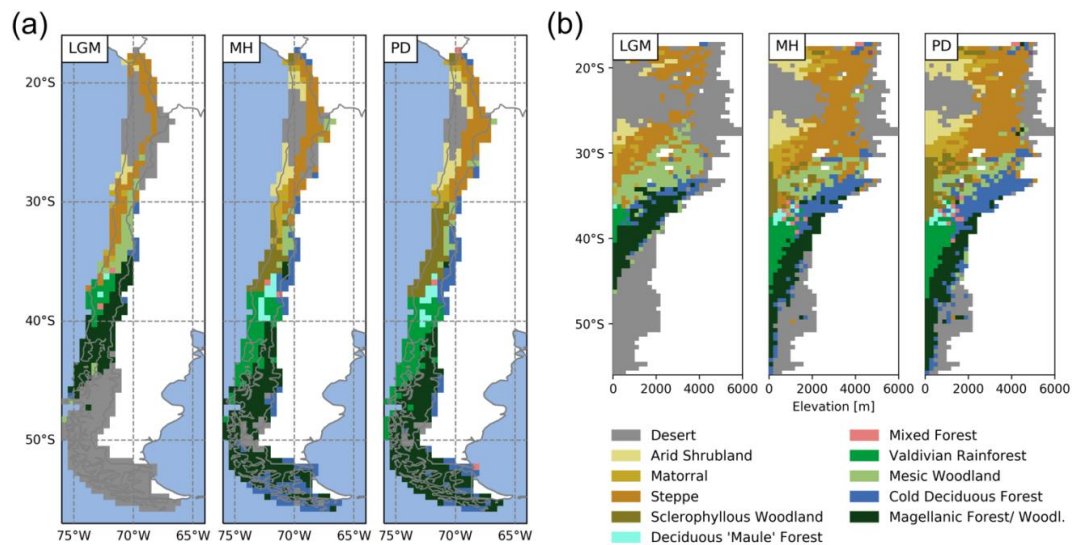
Figure 5. (a) Spatial and **(b)** altitudinal distribution of biomes for Last Glacial Maximum (LGM), Mid Holocene (MH) and present day (PD) (for biome classification decision tree see Fig. B1).
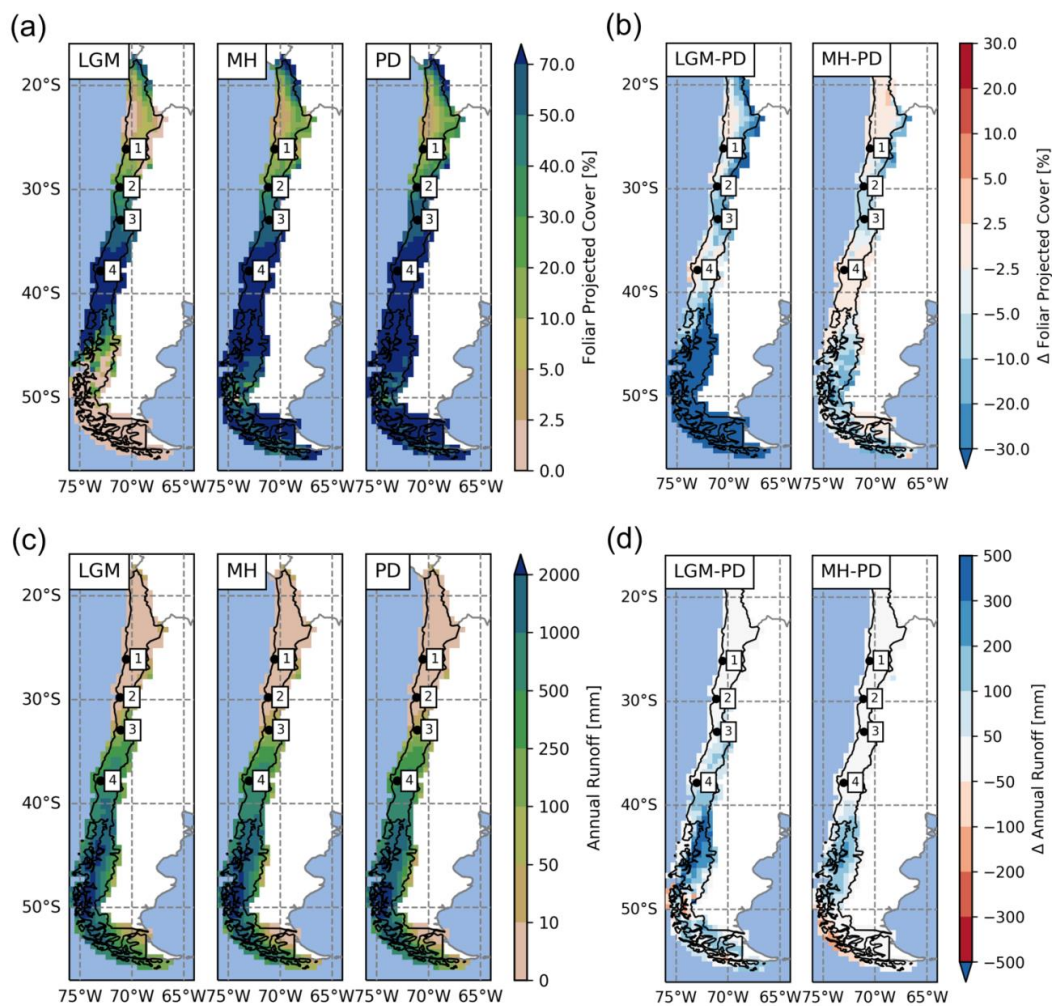
Figure 6. Spatial distribution of **(a)** foliar projected cover and **(c)** surface runoff simulated for Last Glacial Maximum (LGM), Mid Holocene (MH) and present day (PD). **(b)** and **(d)**: difference plots of LGM vs. PD (left) and MH vs. PD (right) for foliar projected cover and runoff, respectively (1: Pan de Azúcar, 2: Sta. Gracia, 3: La Campana, 4: Nahuelbuta).
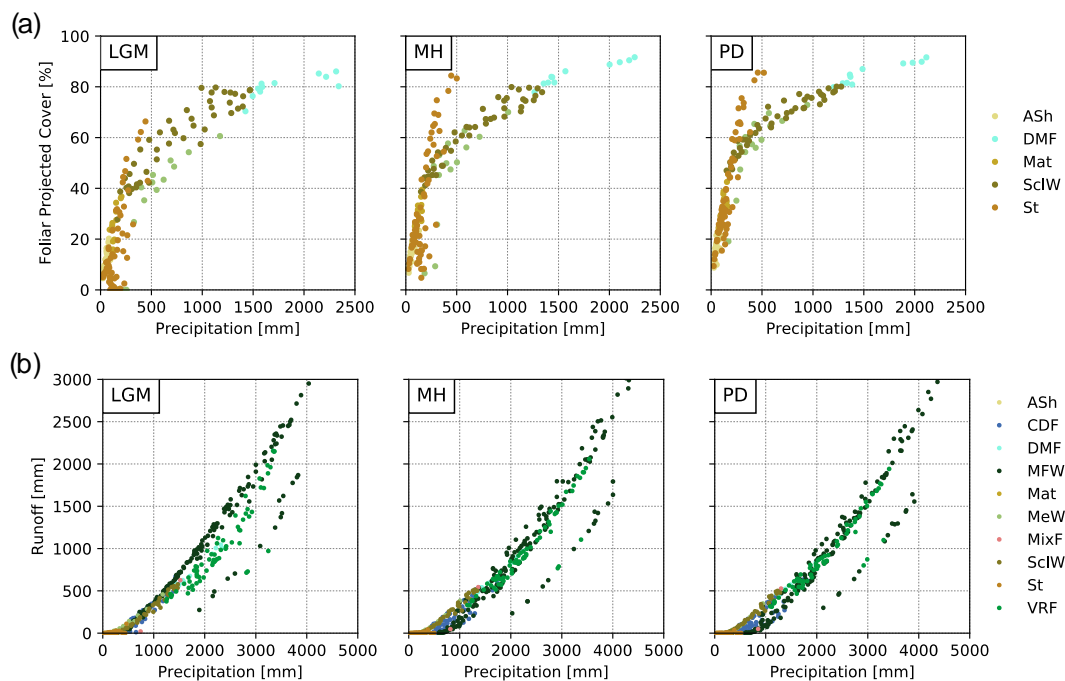
Figure 7. (a) Foliar projected cover (FPC) and **(b)** surface runoff as a function of annual average rainfall for Last Glacial Maximum (LGM), Mid Holocene (MH) and present day (PD) (ASh: *Arid Shrubland*, CDF: *Cold Deciduous Forest*, DMF: *Deciduous 'Maule' Forest*, MFW: *Magellanic Forest/ Woodland*, Mat: *Matorral*, MeW: *Mesic Woodland*, MixF: *Mixed*

5 *Forest*, SclW: *Sclerophyllous Woodland*, St: *Steppe*, VRF: *Valdivian Rainforest*; temperate and boreal forest biomes (CDF, MixF, VRF, MFW) excluded from subplot (a) as they are also strongly dependent on temperature.
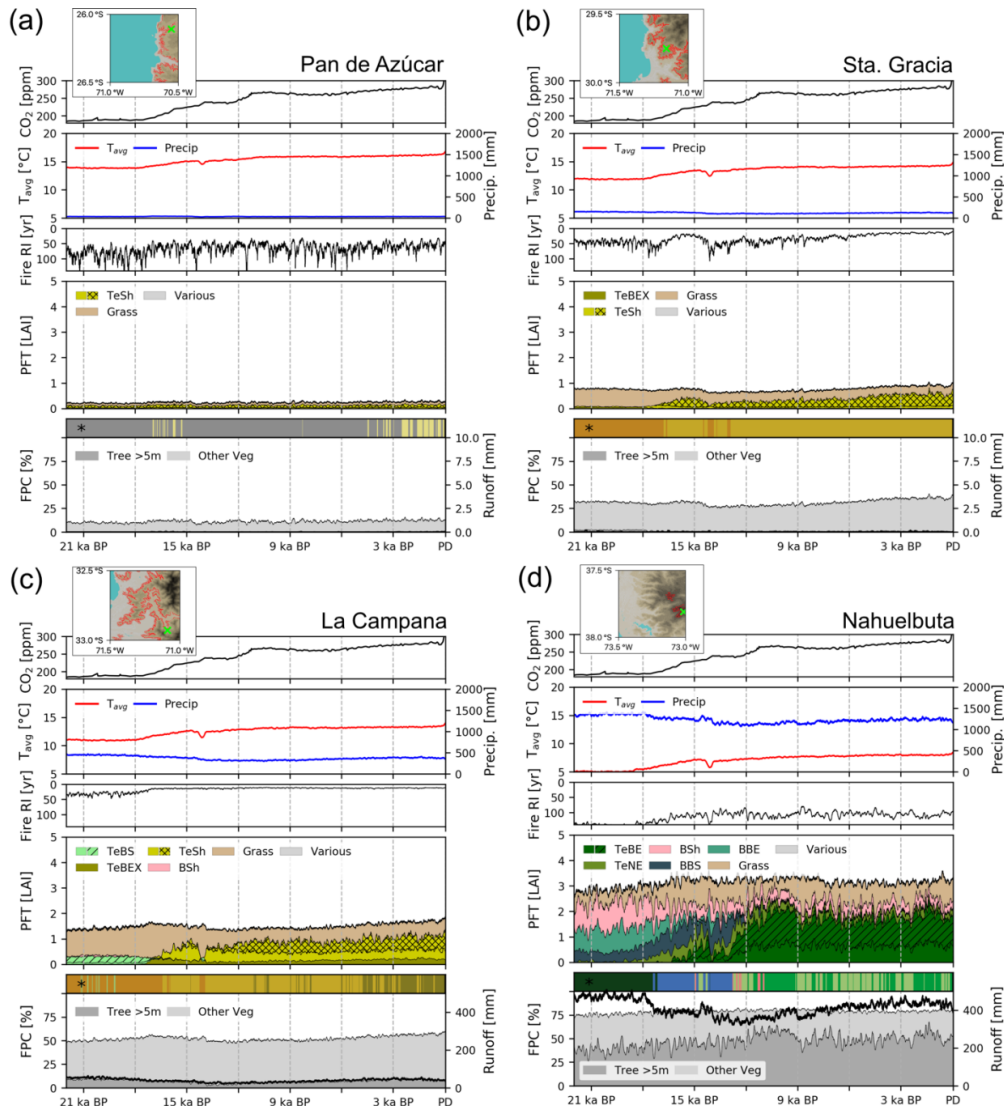
Figure 8. Transient simulations for the sites **(a)** Pan de Azúcar (a), **(b)** Sta. Gracia, **(c)** La Campana, and **(d)** Nahuelbuta. The insets show the location within the simulated 0.5°x0.5° grid cell and the area and location covered by the landform plotted in this figure (results given in other figures are an area-weighted aggregation of individual landform simulation results). Panels 1-3: T_{avg}: annual average temperature, Precip: annual precipitation, Fire RI: fire return interval. Panel 4: PFT: plant function type, (grouped) PFT abbreviations: TeSh (temperate shrub), Grass: herbaceous vegetation, TeBEX: sclerophyllous temperate broadleaved evergreen tree, TeBS: temperate broadleaved summergreen tree (hashed: shade-intolerant), BSh: boreal evergreen shrub, TeBE: temperate broadleaved evergreen tree, TeNE: temperate needleleaved evergreen tree, BBS: boreal broadleaved summergreen tree, BBE: boreal evergreen tree, Various: other PFTs (LAI < 0.05); plain: shade-intolerant, hatched: shade-tolerant, cross-hatched: raingreen. Panel 5: FPC: foliar projected cover, classification: trees and shrubs >5m (darkgray), herbaceous vegetation and small trees and shrubs (light gray); Runoff: simulated surface runoff; *) Biomization: for a legend on the applied classification see Fig. B1 and Fig. 4 for a color-coded legend. All data smoothed using 100-year averaging.
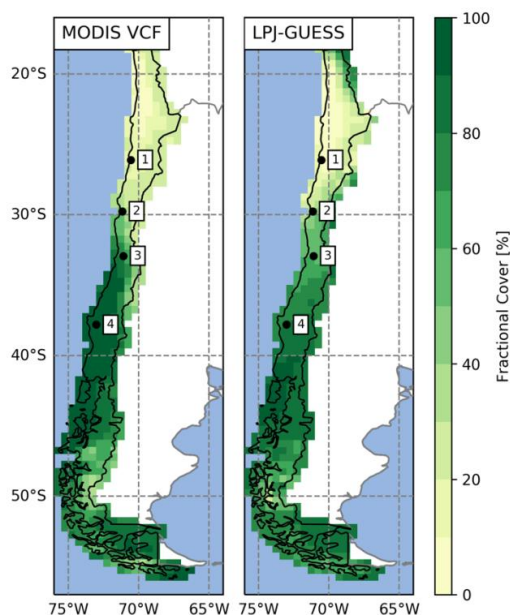
Figure 9. Comparison of satellite-derived vegetation cover and simulated average foliar projected cover of potential natural vegetation for present day (data: MODIS MOD44B VCF v6, total vegetation, 2001-2016 average; Townshend, 2017; 1: Pan de Azúcar, 2: Sta. Gracia, 3: La Campana, 4: Nahuelbuta).
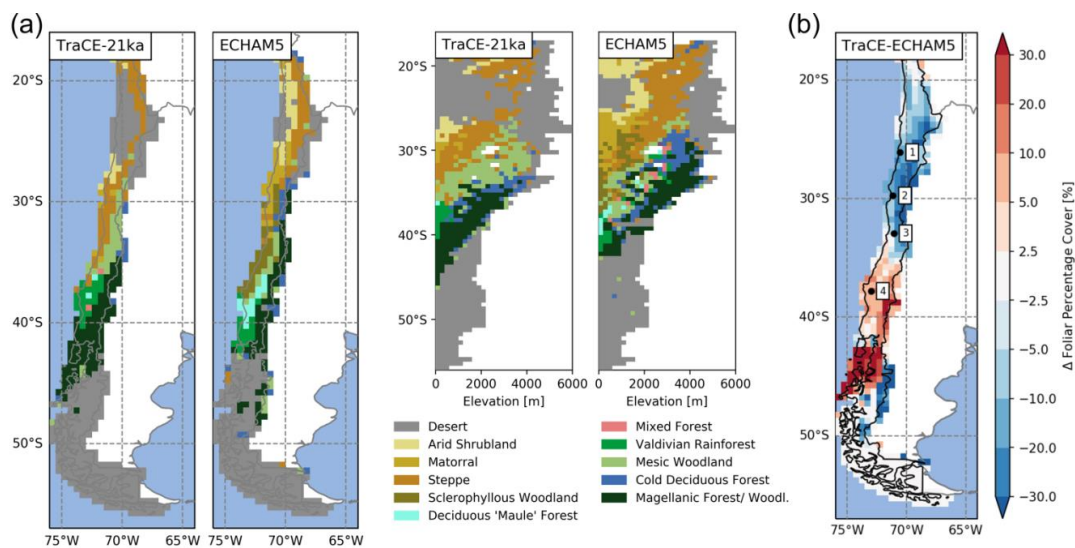
Figure 10. (a) Effect of paleoclimate input data used for LPJ-GUESS simulations on the spatial and altitudinal biome distribution and **(b)** effect on simulated foliage projected cover (given as difference between TraCE-21ka simulation and ECHAM5 simulation results, Mutz et al., 2017). For a comparison of differences between average temperatures and precipitation between the two climate datasets see Fig. 3 and Fig. S3. 1: Pan de Azúcar, 2: Sta. Gracia, 3: La Campana, 4: Nahuelbuta.
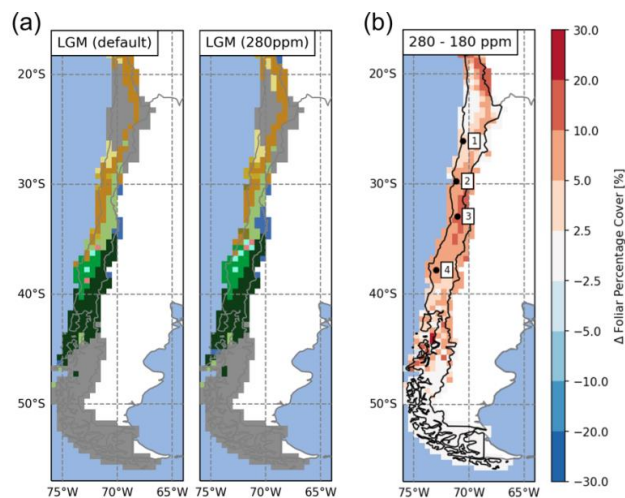
Figure 11. (a) Effect of atmospheric CO_2 ([CO_2]) concentrations on the simulated distribution of biomes for Last Glacial Maximum (LGM) time-slice simulations (left panel: default LGM setup of this study with [CO_2] = 180 ppm, right panel: control run with pre-industrial [CO_2] = 280ppm). **(b)** Difference plot of resulting foliar projected cover (280 ppm − 180 ppm). 1: Pan de Azúcar, 2: Sta. Gracia, 3: La Campana, 4: Nahuelbuta.

Appendix A: Calculation of Monthly Wet Days

It is a well-documented problem that climate models, such as CCSM3, have a tendency to overestimate the precipitation frequency in dry regions (e.g. Dai, 2006). Therefore, we parameterize the number of "wet days" (number of days in a month with rainfall greater than 0.1 mm day^{-1}) based on ERA-Interim daily climatology. It is assumed that the daily precipitation in a month follows a Gamma distribution, which is determined by the shape and scale parameters (α and β, respectively) as:

$$\begin{aligned} \alpha &= (x_{mean}/x_{std})^2, \\ \beta &= x_{std}^2/x_{mean} \end{aligned}$$

where x_{mean} is the monthly mean precipitation, and x_{std} its standard deviation (day-to-day variability). A characteristic feature of the Gamma distribution is its ability to attain two completely shapes depending on the value of α. If $\alpha < 1$ (typical for dry regions), the probability density attains maximum value at zero precipitation and decreases exponentially towards higher precipitation values, and if $\alpha > 1$ (typical for wet regions), the probability density function has a shape more reminiscent of a Gaussian distribution.

The number of wet days is estimated from the cumulative gamma distribution

$$F(x,\alpha,\beta) = \frac{1}{\beta^{\alpha}\Gamma(\alpha)} \int_0^x t^{\alpha-1} \exp(-t/b)dt,$$

where Γ is the Gamma function. The result of this equation is the probability that an observation will fall in the interval [0 x]. Hence for our purposes, the number of wet days (n_{wet}) is determined by

$$n_{wet} = n_{day}(1 - F(x_t,\alpha,\beta))$$

where n_{day} is the number of days in a month, and x_t the threshold value for a wet day (0.1 mm/day).

In our experiments the TraCE-21k climatology influences monthly n_{wet} by modifying x_{mean} at each grid cell. However, due to the poor representation of precipitation frequencies in the TraCE-21ka data, we use a monthly climatology of x_{std} calculated from ERA-Interim.

Appendix B: Plant Functional Type setup and biomization scheme

Table B1. Plant Functional Type (PFT) characteristics used in this study. Climate classes are associated with differing photosynthesis optimum temperatures and base respiration rates (see Smith et al., 2001; Te: temperate, B: boreal; M: Mediterranean was newly introduced with PS temperatures min: 0, low: 17, high: 27, max: 40; resp. coefficient: 1.0). k_{allom1} = constant in allometry equations (Smith et al., 2001; higher values equal wider crowns); $T_{c,min}$ = minimum coldest-month temperature for survival; $T_{c,max}$ = maximum coldest-month temperature for establishment; GDD_5 = minimum degree-day sum above 5 °C for establishment; $fAWC$ = minimum growing-season (daily temperature > 5°C) fraction of available soil water holding capacity in the first soil layer; r_{fire} = fraction of individuals surviving fire; $k_{la:sa}$ = leaf area to sapwood cross-sectional area ratio; z_1 = fraction of roots in first soil layer (the reminder being allocated to second soil layer); a_{leaf} = leaf longevity; a_{ind} = maximum, non-stressed longevity; CA_{max} = maximum woody crown area. r: base respiration rate (modified after Hickler et al., 2012).

PFT	Climate	r (g C g N⁻¹ d⁻¹)	Lifeform	k_{allom1}	$T_{c,min,s}$ (°C)	$T_{c,min}$ (°C)	$T_{c,max}$ (°C)	T_{wmin}	GDD_5 (°C d)	$fAWC$	Shade tol.	r_{fire}	$k_{la:sa}$	z_1	a_{leaf} (yr)	a_{ind} (yr)	CA_{max} (m²)
TeBE$_{tm}$	Te	0.055	tree	250	-1	0	15		900	0.3	tolerant	0.1	6000	0.7	2.0	500	30
TeBE$_{itm}$	Te	0.055	tree	250	-1	0	15		900	0.3	intolerant	0.1	6000	0.7	2.0	400	30
TeBE$_{itscl}$	Te/ M	0.055	tree	250	1	4	18.8		2400	0.01	intolerant	0.5	4000	0.5	2.0	250	30
TeBS$_{tm}$	Te	0.055	tree	250	-14	-13	6	5	1800	0.3	tolerant	0.2	6000	0.6	0.5	500	30
TeBS$_{im}$	Te	0.055	tree	250	-14	-13	6	5	1800	0.3	intolerant	0.2	6000	0.6	0.5	400	30
TeE$_s$	Te/ M	0.055	shrub	100	1	1	-		2600	0.001	intolerant	0.5	3000	0.5	2.0	100	10
TeR$_s$	Te/ M	0.055	shrub	100	1	1	-		2800	0.001	intolerant	0.5	3000	0.5	1.0	50	10
TeNE	Te	0.055	tree	150	-7	-7	22		600	0.3	intolerant	0.5	5000	0.7	2.0	400	30
BBS$_{tim}$	B	0.11	tree	250	-30	-30	3		150	0.1	intolerant	0.1	6000	0.6	0.5	300	30
BBE$_{tim}$	B	0.11	tree	250	-30	-30	5		250	0.5	intolerant	0.1	6000	0.8	2.0	400	30
BE$_s$	B	0.11	shrub	100	-	-	4.5		150	0.3	intolerant	0.1	2000	0.8	2.0	50	10
C3G	-	0.055	herbac.	-	-	-	-		-	0.1	-	0.5	-	0.9	0.75	-	-

Figure B1. Flowchart of the decision tree used to classify plant functional types (PFTs) into biomes. LAI_{TOT}: LAI of all PFTs; LAI_T: LAI of tree PFTs; LAI_W: LAI of trees + shrubs; LAI_G: LAI herbaceous PFT; LAI_X: LAI of xeric PFTs; LAI_B: LAI of boreal PFTs; $fLAI_n$: fraction of LAI pf PFT_n versus its peers (all tree PFTs, boreal PFTs, etc.); TeBE: temperate broadleaved evergreen tree; TeBS: temperate broadleaved summergreen tree; BBE: boreal broadleaved evergreen tree; BBS: boreal broadleaved summergreen tree.